thermo

MDPI

Article

Experimental Study of Aqueous Foam Use for Heat Transfer Enhancement in Liquid Piston Gas Compression at Various Initial Pressure Levels

Barah Ahn, Macey Schmetzer and Paul I. Ro *

Department of Mechanical Engineering, Baylor University, One Bear Place #97356, Waco, TX 76798-7356, USA
* Correspondence: paul_ro@baylor.edu

Abstract

The acceleration of climate change and increasing weather-related disasters require more active utilization of renewable energy. To maximize the use of renewable energy, energy storage is an essential part. Liquid piston gas compressors have recently drawn attention because of their applicability to compressed air-based energy storage. Aqueous foam can be used to enhance the efficiency of liquid piston gas compression by boosting heat transfer. To validate the effectiveness of the combination of liquid piston and aqueous foam in a multi-stage compression system, which can contribute to higher efficiency, the present work performed experimental study at various pressure levels. Compressions were performed with and without aqueous foam at three different initial pressure levels of 1, 2, and 3 bars. For each cycle of compression, a pressure ratio of 2 was used, and the impact of pressure levels on compression efficiency was measured. With the use of foam, isothermal efficiencies of 91.4, 88.2, and 86.6% were observed at 1, 2, and 3 bar(s), which improved by 2.2, 2.1, and 1.3% compared to the baseline compressions. To identify the cause of the effectiveness variations, the volume changes in the foam at the different pressure levels were visually compared. In higher-pressure tests, a significant reduction in the foam amount was observed, and this change may contribute to the decreased effectiveness of the technique.

Keywords: compressed air energy storage; liquid piston; heat transfer enhancement; aqueous foam

check for updates

Academic Editor: Marcello Iasiello

Received: 15 August 2025
Revised: 29 September 2025
Accepted: 30 September 2025
Published: 3 October 2025

Citation: Ahn, B.; Schmetzer, M.; Ro, P.I. Experimental Study of Aqueous Foam Use for Heat Transfer Enhancement in Liquid Piston Gas Compression at Various Initial Pressure Levels. *Thermo* **2025**, *5*, 39. https://doi.org/10.3390/thermo5040039

Copyright: © 2025 by the authors. Licensee MDPI, Basel, Switzerland. This article is an open access article distributed under the terms and conditions of the Creative Commons Attribution (CC BY) license (https://creativecommons.org/licenses/by/4.0/).

1. Introduction

One of the main contributors to climate issues is greenhouse gas emissions that result from excessive use of fossil fuels. The percentage of the world's energy generation supplied by fossil fuels is gigantic [1]. For instance, in 2022, about 60% of the electricity was generated from the use of fossil fuels in the United States [2]. To prevent a continual increase in global warming, there is a worldwide demand for the reduction in the massive use of fossil fuels. Replacing some portion of fossil fuel energy generation with renewable energy can help with mitigating greenhouse gas emissions. However, the intermittent characteristics of the energy from renewable sources complicate their utilization [3,4]. Storing unused energy when the generation is active and using it in on-peak hours is a strategy to neutralize the issue [5]. Considering various factors such as expense, duration, and capacity, pumped hydroelectric storage (PHS) and compressed air energy storage (CAES) are viewed as promising large-scale energy storage options [6]. PHS requires reservoirs with different

elevations, a specific geological feature which limits the availability of the system. Even though a traditional CAES system also demands a specific geological feature for a storage vessel such as an underground cavern [7,8], various approaches to utilizing the technology in diverse conditions have been made and are expected to enhance the availability of CAES. Building an artificial storage structure for a small size CAES is one possibility. For example, a storage tank composed of tiered pipes was suggested to improve the geological flexibility [9]. For ocean/underwater-based CAES, taking advantage of a bag-type storage vessel [10], a container installed on a seabed [7], and saline aquifers [11] have been suggested as a storage tank. Given that coupling CAES with renewable sources has been discussed in many studies [5,12–14], CAES can be viewed as one of the promising options for renewable energy storage applications. Nevertheless, it has a critical disadvantage of relatively low efficiency. The cycle efficiencies of the two widely known commercialized CAES plants in Huntorf, Germany, and McIntosh, Alabama, are 42% and 54%, respectively [15]. One cause of this energy loss is heat generation during the air compression stage, due to the increased kinetic energy of air [16]. I-CAES (Isothermal CAES) is gaining more attention as a technique to minimize energy loss due to heat generation [17,18]. The concept of I-CAES is to maximize heat transfer during the compression/expansion processes, which lead to an isothermal process [19,20]. In an ideal isothermal process, there is no temperature change during compression. Given that some of the newly proposed CAES concepts are dependent on the isothermal process [5,11,21,22], achieving a near-isothermal process plays a critical part in the further development of CAES system.

The liquid piston gas compressor has been studied by many due to its potential for energy storage applications. The main concept of a liquid piston is that a liquid column serves as the compressing piston of a conventional gas compressor. The conformity of liquid enables diverse heat transfer enhancement techniques to be incorporated [19,23,24]. Additionally, putting an insert into the chamber to provide an additional contact area was widely studied. In [25], two types of porous media inserts, interrupted plates and metal foam, with different dimensional parameters, were experimentally tested. With the use of inserts, compression efficiency was increased at a fixed power, and vice versa. The porous media application with widely extended pressure range was examined in [26]. The advantages of porous inserts were validated in the pressure range up to 210 bars, and the optimal location of a porous insert was examined. A compression technique that has a similar working mechanism to a liquid piston was studied in [27–29], and it was proven that the combination of porous media and a liquid is beneficial for compression efficiency improvement. Other than porous media, parallel metal plate inserts [30] and metal wire mesh [31] were used with a liquid piston, and they also reduced the temperature changes.

Apart from heat transfer enhancing technologies using a solid insert, liquid-based techniques for heat transfer enhancement have been investigated as well. Spray injection is a representative and intuitive liquid-based method. Water droplets are injected through a spray nozzle and provide extra surface area for heat transfer. In [20], a parametric study was performed via simulation. The type of spray injection, water mass, and droplet size were varied, and their impacts on the isothermal performance were evaluated. In [32], the pressure and nozzle angle of spray were varied, and their impacts were tested. The spray was operated at pressures varying from 10 PSI to 70 PSI with 10 PSI intervals. The higher the spray pressure is, the smaller the temperature changes the air experiences. This is because of the larger flowrate that results from the higher-pressure operation. However, higher pressure does not actually lead to better efficiency due to the extra work input required for spray. A more detailed analysis of the droplet heat transfer was performed in [33] to extend the understanding of the method. The heat transfer coefficient of a single

droplet was estimated based on spray parameters, and the importance of spray parameters in determining the heat transfer was highlighted.

In addition to integrating heat transfer enhancement techniques, performing compression via a multi-stage system is key to increasing the system efficiency. Figure 1 displays pressure–volume trajectories of the isothermal, single-stage, and multi-stage compressions.

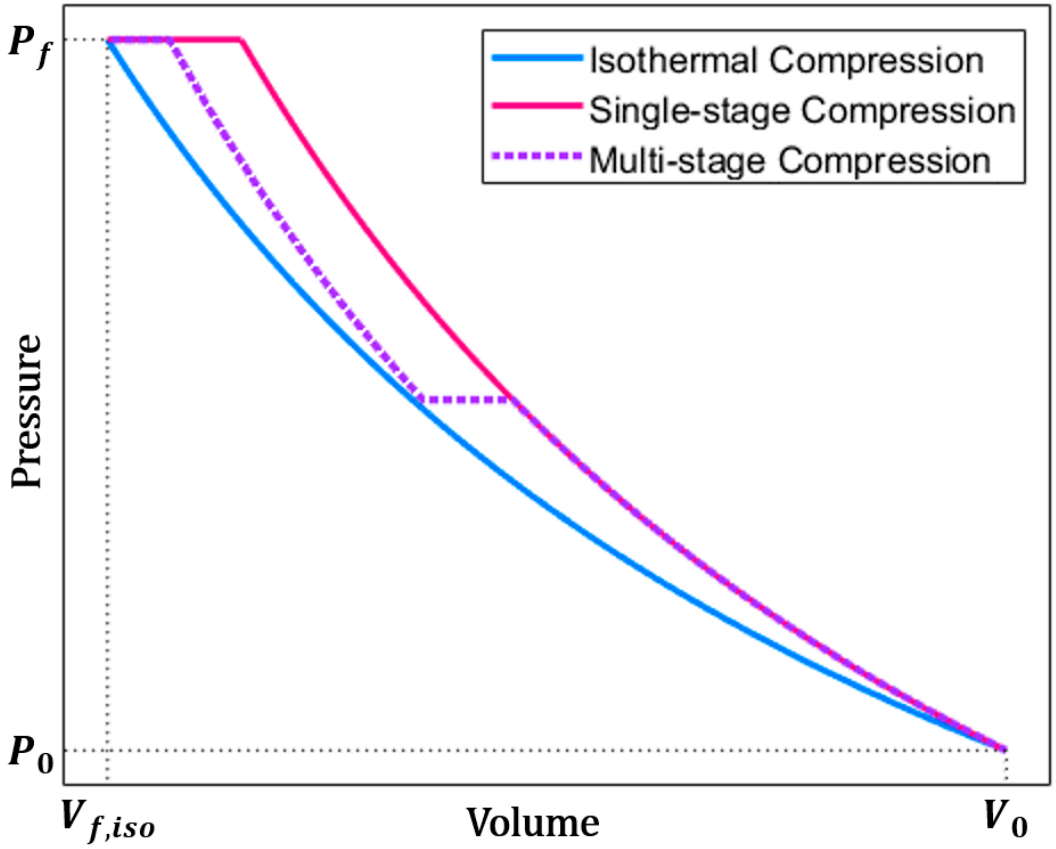


Figure 1. Work consumption comparison between single and multi-stage compression.

By computing the area under a trajectory that starts from the initial point of (V_0,P_0) and ends at the target point of ($V_{f,iso}$,P_f), the work input of a process can be determined. As shown in Figure 1, compression conducted along the trajectory labeled as multi-stage compression consumes less work than compression along the single-stage compression trajectory by taking an intercooling step. In a multi-stage compression process, because a single process is split into two compression cycles, each cycle has a different pressure level. Therefore, testing at various pressure levels is key to evaluating actual applicability of liquid piston gas compression, and there have been studies on this topic.

The impact of initial pressure levels on isothermal compression performance of a liquid piston has been experimentally studied [33,34]. Under consistent conditions, higher initial pressure resulted in a decline in isothermal performance. This is because of the greater amount of heat generation while heat transfer conditions remained the same [34]. Taking into consideration the air dissolution, the impact of pressure levels can be more significant [33]. Spray injection technique with a liquid piston compressor was tested at various pressure levels to examine its applicability to a multi-stage compression system [35].

In addition to the spray injection, aqueous foam is another liquid-based method to increase heat transfer in a liquid piston. Comparing the experimental results of liquid-based techniques, spray and aqueous foam, presented in [32,36,37], the spray injection method showed a better isothermal performance under the test conditions. However, the tests were conducted starting from atmospheric pressure. For application to an actual CAES system,

where compression starts at various initial pressure levels due to multi-stage compression, this trend may differ due to additional work consumption of the spray method. This is particularly because the spray technique requires the injection throughout the entire stroke time or for an extended time. On the contrary, the fundamental concept of the aqueous foam technique is to fill the compression chamber with the foam prior to the start of the compression process. Because the foam serves as a surface area for heat exchange, the temperature changes during the compression can be abated. Because the foam generation is required only ahead of the compression, it has a relative advantage of requiring no extra work input while the compression is ongoing. A parametric study was performed to examine the impact of the volume of the foam filling the compression chamber, flowrate of air to generate the foam, and foam generator design in [36]. Other than this specific article, it is hard to find another related literature about the foam application to energy storage. An ICAES project that takes advantage of aqueous foam [38] was occasionally mentioned in the research literature [27,36,39] and online articles [40–43]. According to their technology report [38], the project successfully operated a foam-based air compression system for energy storage with isothermal efficiency higher than 95%. However, no follow-up work can be found. Although there have been studies on the heat transfer features [44,45] and rheology of a foam flow [46,47], it is hard to apply their analytical models to the current study. This is because the behavior of aqueous foam in a compressor cannot be viewed as a typical foam flow. Hence, there is a need for additional studies to improve the understanding of the use of aqueous foam in a liquid piston.

The purpose of the current study is to extend the understanding of the former aqueous foam study of [36]. Because the previous aqueous foam tests of [36] were limited to a process starting from the atmospheric pressure, it has not yet been identified whether the technique maintains its value as a heat transfer booster at a higher pressure level, which is a critical issue in an actual CAES system. The current paper consists of five sections. The first section introduces the background and the current state of the topic. In the second section, analytical models to mathematically describe the process are suggested. The next section illustrates the methodology of the experiment, which is followed by a presentation and discussion of the results. Then, the final section gives the conclusion.

2. Analytical Modeling

The energy equation based on the first law of thermodynamics has been used to express the liquid piston gas compression [31–33,48,49]:

$$\dot{U} = \dot{Q} - \dot{W}_{compression} \tag{1}$$

Alternative expressions of the three terms of Equation (1) allow the equation to be rewritten as follows:

$$m_{air} C_v \frac{dT_{air}}{dt} = U_h A_s (T_\infty - T_{air}) - P_{air} \frac{dV_{air}}{dt} \tag{2}$$

Because the volume of air decreases and air temperature increases, the heat transfer rate term has a negative value while the compression work rate term, $-P_{air}\frac{dV_{air}}{dt}$, has a positive value. The right-hand side is equivalent to the difference in the absolute values of the compression work rate term and the heat transfer rate term [48]. A smaller value of the right-hand side leads to a smaller temperature change in the left-hand side. Since the compression work rate term typically has a greater value than the heat transfer rate term, the addition of extra heat transfer term helps make the right-hand approach zero, which is an ideal isothermal compression process. With the introduction of aqueous foam, another heat transfer rate term, $\dot{Q}_{foam}$, is added to the right-hand side. As a result, the

energy equation for the liquid piston air compression with aqueous foam can be written as Equation (3).

$$m_{air}C_v\frac{dT_{air}}{dt} = U_hA_s(T_\infty - T_{air}) + \dot{Q}_{foam} - P_{air}\frac{dV_{air}}{dt} \quad (3)$$

There have only been a limited number of studies that delve into the aqueous foam application to air compression. To the author's best knowledge, the research in [36] is the only article that studied aqueous foam application to liquid piston gas compression. The article brought an analytical expression of single-phase power-law fluid flow through a pipe to depict the aqueous foam heat transfer. The expressions of Nusselt number of foam flow used in [36] are given in Equations (4) and (5).

$$Nu_X = 1.41\left(\frac{3k+1}{4k}\right)^{\frac{1}{3}}\left(\frac{D_hRePr}{x}\right)^{\frac{1}{3}} \quad (4)$$

$$Nu_X = \frac{8(5k+1)(3k+1)}{31k^2+12k+1} \quad (5)$$

where k and x are thermal conductivity and length coordinate.

However, in liquid piston compression, because the finite chamber height limits the stroke length of the piston, it may be erroneous to consider the aqueous foam behavior as a typical foam flow through a pipe. Furthermore, the rise in the pressure and temperature of the chamber caused by compression results in considerable collapse of the foam. Hence, the amount of foam existing in the chamber decreases with the progress of compression, which makes the foam behavior in the liquid piston compression different from a typical foam flow through a pipe. More importantly, the primary interest of this application is not the heat transfer of the two-phase flow itself, but the heat exchange between the foam and air, which are the components of the flow. Thus, another suggestion for the foam heat transfer modeling needs to be proposed.

Figure 2 schematically shows the heat transfer model of liquid piston air compression with aqueous foam. The heat transfer between the air layer and the surroundings is the same as the heat transfer model of the baseline compression (compression without foam use) except that the bottom of the air layer is in contact with the foam surface instead of the water surface. Hence, no extra heat transfer element is needed for the air layer portion. There are two parts of heat transfer within the foam layer: heat transfer between the air and the bubble surface, and between the air and the chamber wall (labeled as Foam Heat Transfer #1 and #2 in Figure 2). For Foam Heat Transfer #1, it is reasonable to presume that the heat transfer between the air trapped in a bubble and the surface of the bubble is conduction. This is because the air trapped in a bubble moves up altogether with the bubble as the liquid piston rises during the compression. For Foam Heat Transfer #2, there may be a convective heat transfer taking place between air trapped between the wall and the bubble surface. However, the convective heat transfer between the chamber wall and the air near the wall is not a new component, in that it takes place in the baseline process as well. Also, there may be a convective heat transfer between the bubble surface in contact with the wall as the bubble rises up the wall due to compression, which could be a part of Foam Heat Transfer #2. However, our experience from the earlier work [36] confirms that this is negligible. Therefore, the additional heat transfer rate term, $\dot{Q}_{foam}$, can be identified as conductive heat transfer between the air trapped in a bubble and the bubble surface. The heat transfer rate of a single bubble can be written as Equation (6).

$$\dot{q}_{foam} = k_{foam}A_{foam}\frac{\left(T_{foam} - T_{air}\right)}{L_{foam}} \quad (6)$$

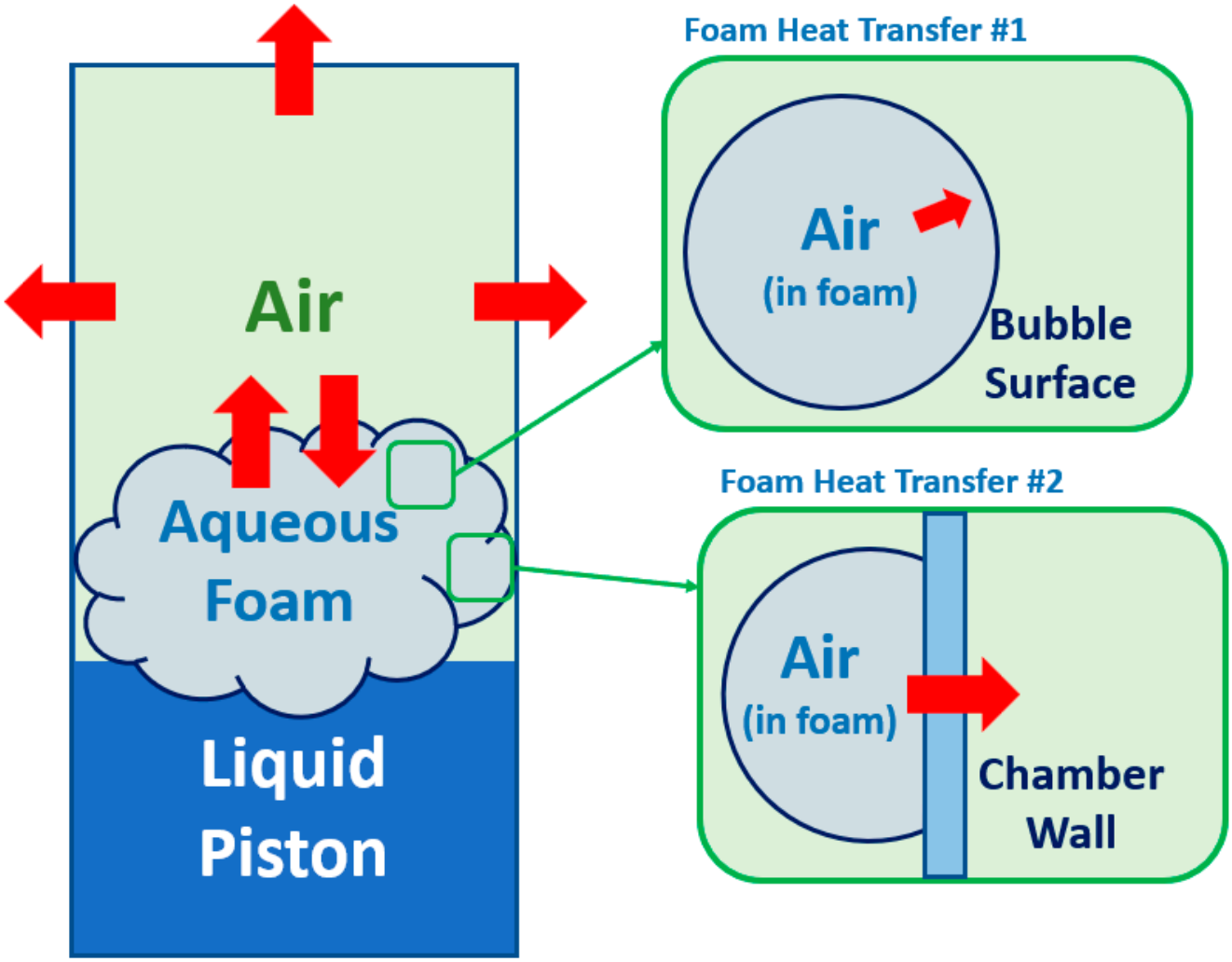


Figure 2. Heat transfer diagram of aqueous foam in liquid piston.

Then, the foam heat transfer term, $\dot{Q}_{foam}$, can be expressed as the sum of each bubble. In Equation (7), i indicates i^{th} bubble and the characters with the subscription i means the properties of i^{th} bubble.

$$\dot{Q}_{foam} = \sum_{i=1}^{N} \left(k_{foam,i} A_{foam,i} \frac{\left(T_{foam,i} - T_{air} \right)}{L_{foam,i}} \right) \tag{7}$$

Incorporating $\dot{Q}_{foam}$ expression into Equation (3), the energy equation for liquid piston gas compression with aqueous foam can be arranged as Equation (8).

$$m_{air} C_v \frac{dT_{air}}{dt} = U_h A_s (T_\infty - T_{air}) + \sum_{i=1}^{N} \left(k_{foam,i} A_{foam,i} \frac{\left(T_{foam,i} - T_{air} \right)}{L_{foam,i}} \right) - P_{air} \frac{dV_{air}}{dt} \tag{8}$$

Although $\dot{Q}_{foam}$ is modeled with a conductive heat transfer term in an intuitive manner, it is very difficult to express $\dot{Q}_{foam}$ term in a more detailed manner due to the different shape and dimension of each bubble. In addition, the presence of the foam may affect the dynamics of the overall air flow in the chamber. However, because the microscopic observation of how the air flow dynamics change is beyond the scope of the current work, its impact is not reflected in the mathematical models.

The efficiency of the compression process is evaluated based on the isothermal efficiency calculation, which has been commonly used in many liquid piston studies [31,32,36,48–50]. Figure 3 displays the profiles of isothermal, adiabatic, and an actual compression process starting from the initial point (V_0,P_0) to the final point ($V_{f,iso}$,P_f). The compression work can be obtained by calculating the area under a profile. The isothermal process has the smallest area under its profile, whereas the adiabatic process has the largest area. For a non-isothermal profile, when the target pressure, P_f, is achieved, the volume at the point, V_f, is larger than the final volume, $V_{f,iso}$. Then, there needs to be a horizontal move from (V_f,P_f) to ($V_{f,iso}$,P_f), which is a cooling work after compression [32,48–50]. An actual compression profile is generally placed between the profiles of isothermal compression and adiabatic compression. Based on compression profiles, the efficiency of a process can be assessed. The closer a process is to the isothermal profile, the more efficient the process. Efficiency can be numerically evaluated as well. The isothermal compression efficiency, η_{iso}, is determined by comparing an actual compression profile and the isothermal profile in Equation (9).

$$\eta_{iso} = \frac{W_{isothermal}}{W_{comp} + W_{cooling}} = \frac{\overbrace{-\int_{V_0}^{V_{f,iso}} (P_{iso}(V_{iso}) - P_0)dV}^{W_{isothermal}}}{\underbrace{-\int_{V_0}^{V_f} (P(V) - P_0)dV}_{W_{comp}} + \underbrace{P_0(Pr-1)\left(V_f - \frac{V_0}{Pr}\right)}_{W_{cooling}}} * 100\ [\%] \quad (9)$$

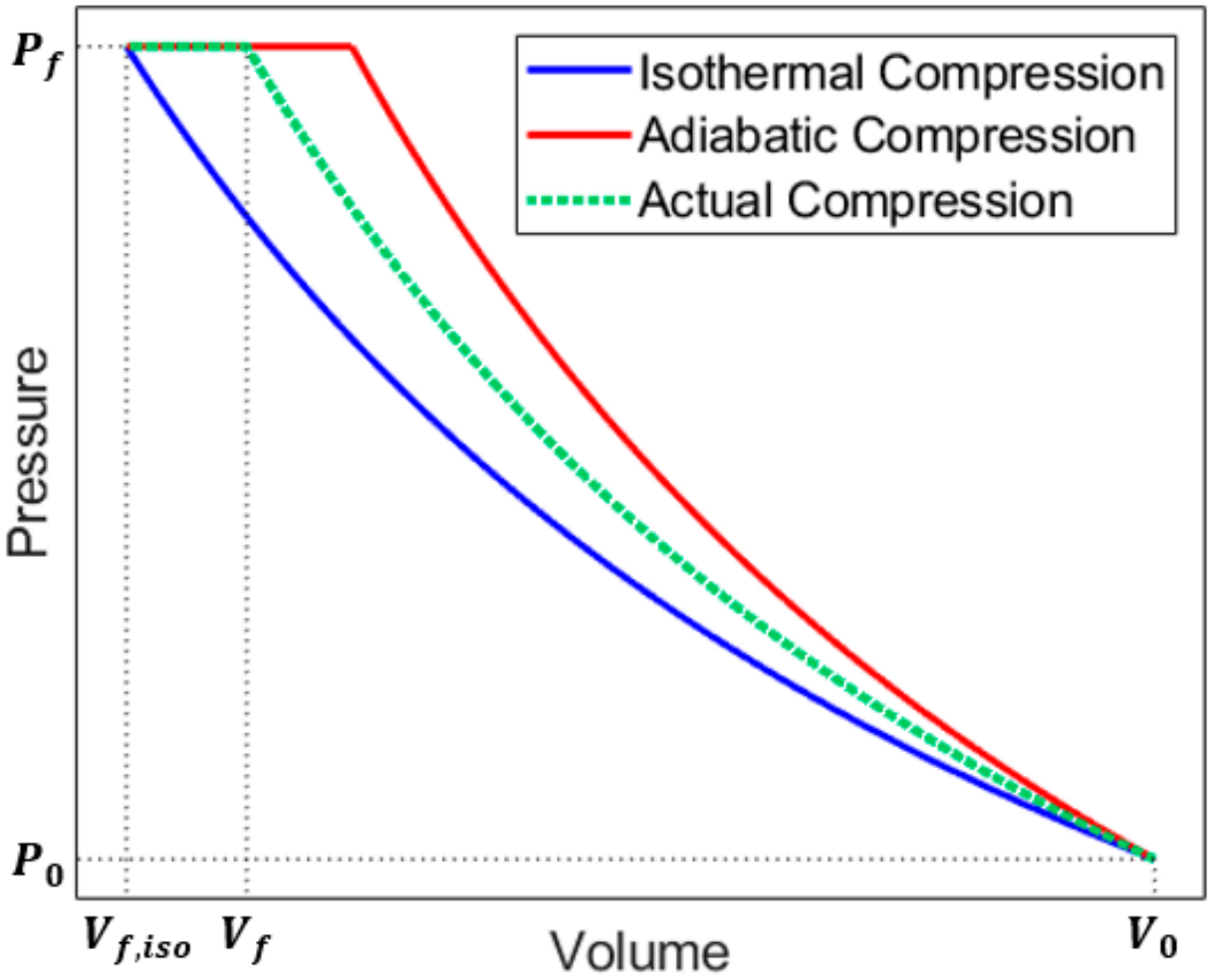


Figure 3. Compression profiles comparison of isothermal, adiabatic, and polytropic processes.

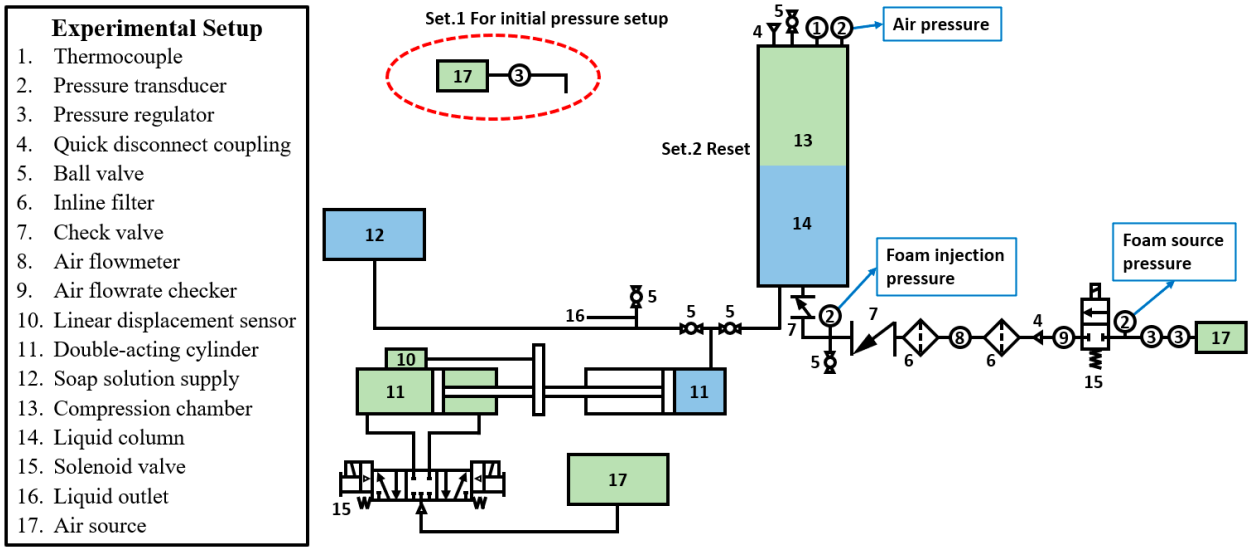
3. Methodology

Figure 4 shows the schematic diagram and an actual picture of the experimental setup. A 2-foot-long polycarbonate cylinder serves as the compression chamber (part #2 of Figure 4a). Since the two ends are closed with aluminum plates and the starting water level is slightly above the floor of the chamber, the actual height occupied by the air is about 574.5 mm. On the top plate, a thermocouple (#1) and a pressure transducer (#2) are installed to measure the temperature and pressure of the air. A quick disconnect coupling (#4) is also located on the top plate. It functions as an outlet to the atmosphere by connecting a plug pipe and can be used as a path for air injection to set up a higher initial pressure by connecting to an air source. In this experimental setup, a soap solution served as the liquid in the liquid piston. This allows aqueous foam to be generated simply by blowing air through the bottom of the chamber. The soap solution was prepared by manually shaking water and a commercialized dishwashing-detergent. In this work, the primary goal is to observe general heat transfer trends at different pressures. Since the concentration of the solution is not a parameter of interest in this study, a random amount of the detergent sufficient to generate aqueous foam was used to make one batch of solution, which was used throughout the entire experiments without changing. Two double-acting cylinders (#11) worked as a water pump to carry out compression. The rod ends of the cylinders are coupled and move together, so that the retraction of one cylinder results in the extension of the other. The cylinder directly connected to the chamber is filled with liquid when it is extended. During the compression process, the extension of the other cylinder leads to the retraction of the cylinder connected to the chamber, which pushes the liquid into the chamber. Then, the air in the chamber is compressed. In order to measure the volume of air that is present in the chamber, a linear position sensor (#10) measures the position change in the rods of the cylinders (#11), which can be translated to the change in the liquid volume entering the chamber. Then, by subtracting the volume of the liquid entering the chamber from the initial volume of the air, the volume of the air in real time can be computed.

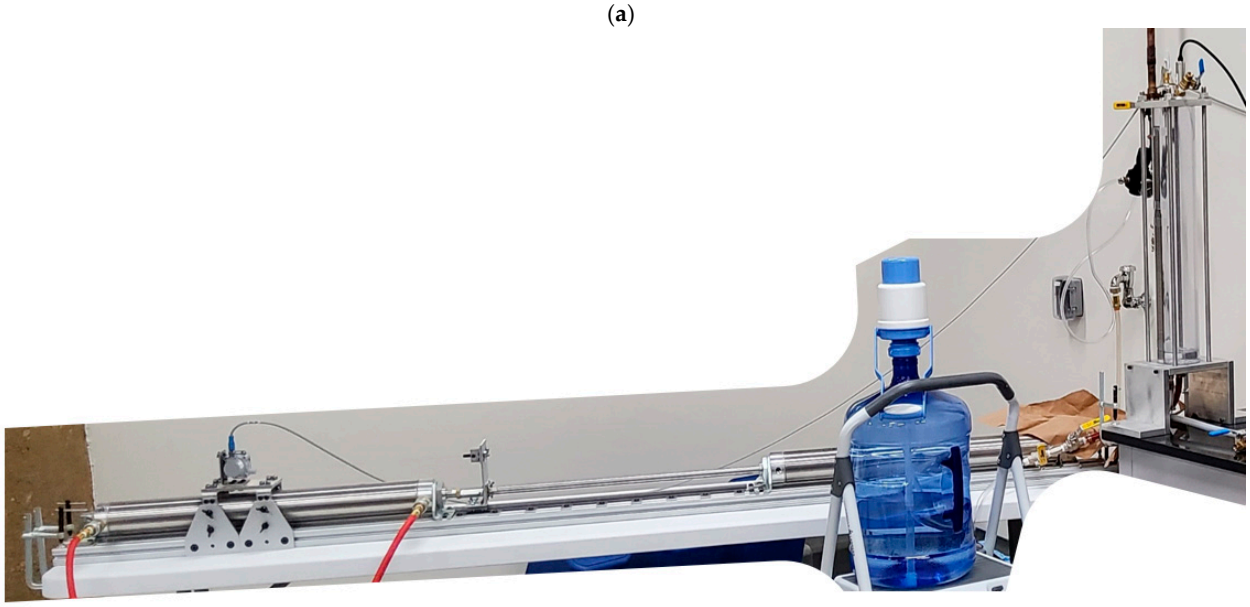
Compressions were conducted with and without aqueous foam at three different pressure levels: 1 bar (atmospheric pressure), 2 bars, and 3 bars. For each case, four strokes of compression were performed with sufficient time intervals between strokes to allow for cooling and a consistent initial condition. For the baseline compression starting at the atmospheric initial pressure, the outlet at the top plate of the chamber (#4) was opened to the atmosphere ahead of each compression stroke to initialize the chamber pressure. For the baseline compression starting at the elevated pressures, air from an air source (#17) was injected into the chamber through the outlet, and the initial pressure was set at 2 and 3 bars first. For the 2 and 3 bar cases, the chamber was set to its initial pressure first, and the outlet remained closed throughout the entirety of the cycle to prevent variation in initial pressures before each stroke. No notable pressure drop was observed, and each stroke started at a constant initial pressure condition due to excellent leakage prevention of the system.

Figure 5 illustrates experimental procedures of compression with aqueous foam. Air is blown into the chamber through the pipe installed at the bottom of the chamber. The pipe is placed one inch away from the radial center of the chamber bottom. For the compression with foam starting at atmospheric pressure, aqueous foam is generated with the outlet on the top of the chamber open to the atmosphere, so that the external air injection to generate the foam does not change the internal pressure of the chamber, and each stroke can start at the atmospheric pressure. Once the chamber is sufficiently filled with foam, the outlet is closed and then compression starts. On the contrary, for the compression starting at elevated pressures, the air is injected with the outlet closed. As a result, the initial pressure increases as well. If the initial pressure setup is performed separately, the same as Baseline-2 and 3, the foam generation process will change the initial pressure level, and the stroke will

not start at its intended initial pressure of 2 and 3 bars. Thus, the foam generation process simultaneously serves as the initial pressure setup by carefully adjusting the air injection time and flowrate to result in a pressure of 2 or 3 bars after foam generation. Because the amount of air needed differs depending on the intended initial pressures, there were slight differences in the amount of foam filling the chamber. Because the detergent served well as a foaming agent, the generated foam stayed without major loss of bubbles during the time interval between strokes once an elevated initial pressure was set.



(**a**)



(**b**)

Figure 4. Liquid piston experimental setup: (**a**) schematic diagram, (**b**) actual picture.

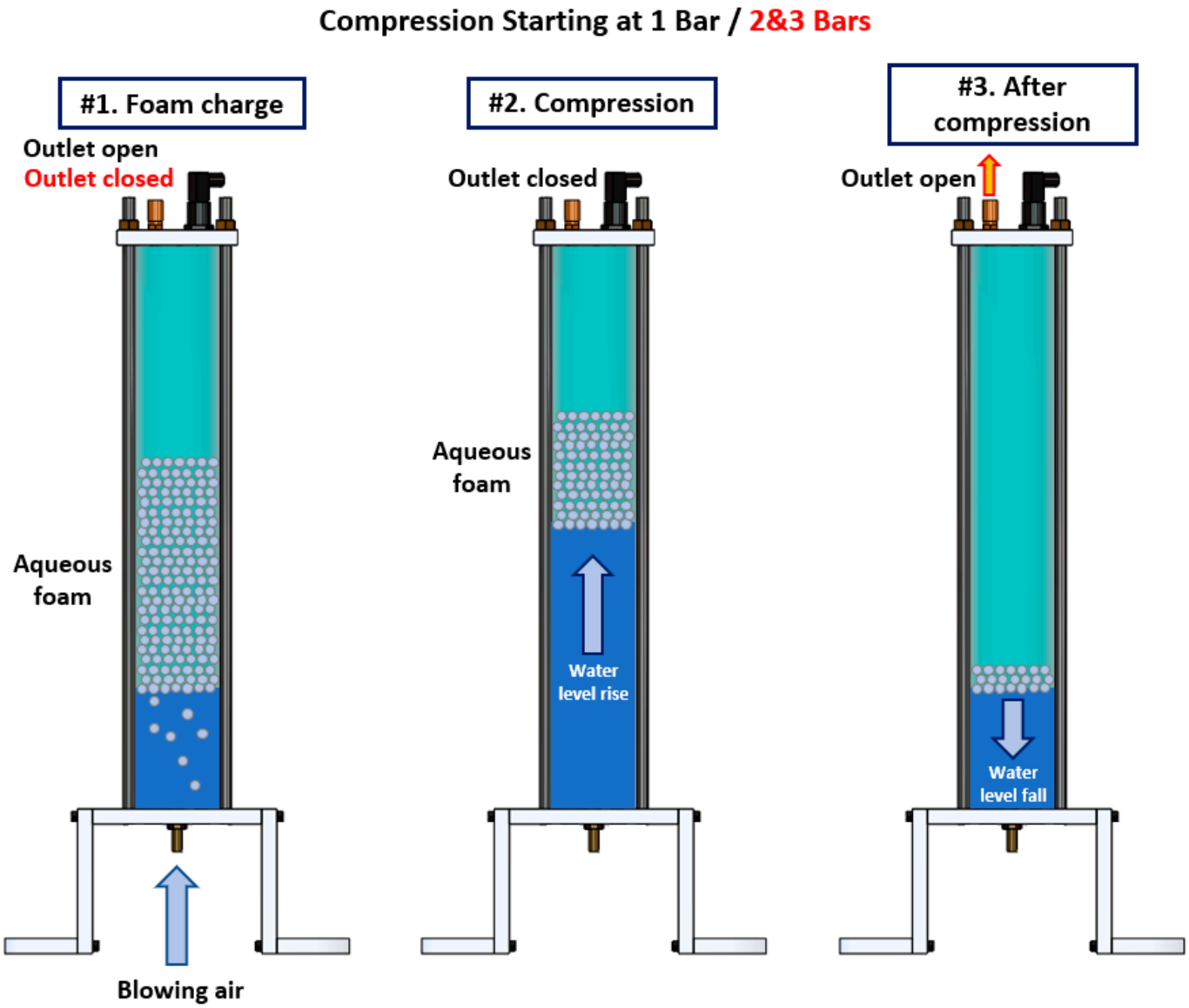


Figure 5. Experimental procedure of compression with aqueous foam.

4. Results and Analysis

4.1. Baseline Compression

To examine the effects of aqueous foam, the baseline compression, a compression process without foam, needs to be performed for comparison. The baseline compressions were conducted at the initial pressures of 1, 2, and 3 bars, with each process referred to as Baseline-1, 2, and 3, respectively.

Figure 6 exhibits the sequence of the baseline experiments by displaying the air pressure of the entire process. Each compression cycle consisted of four strokes, with a resting time between strokes to ensure that each stroke began with consistent initial conditions. This cycle was performed at three different initial pressures: 1 bar (atmospheric pressure), 2 bars, and 3 bars. Data of the last three strokes were collected and averaged for comparison.

Figure 7a–c show the averaged pressure, temperature, and volume of Baseline-1, 2, and 3 up to the point where a pressure ratio of 2 is reached. Although the stroke time of each case was closely matched, the differences were inevitable due to the difficulties of the speed adjustment. A process with higher pressure takes a longer time to reach

the pressure ratio of 2. A slow compression [26,49] is an advantageous condition for the isothermal performance. Therefore, if a process with a higher initial pressure is exposed to a more advantageous condition of a slow compression and still shows a lesser isothermal performance, it is safe to conclude that the process is less efficient than a process with a lower initial pressure. The influence of the initial pressure on isothermal performance can be compared with the temperatures presented in Figure 7b. The temperature increases in Baseline-1, Baseline-2, and Baseline-3 are 28.90 K, 33.32 K, and 36.75 K, respectively. This result agrees with the previous studies [34,48] as a higher initial pressure leads to a reduced isothermal performance.

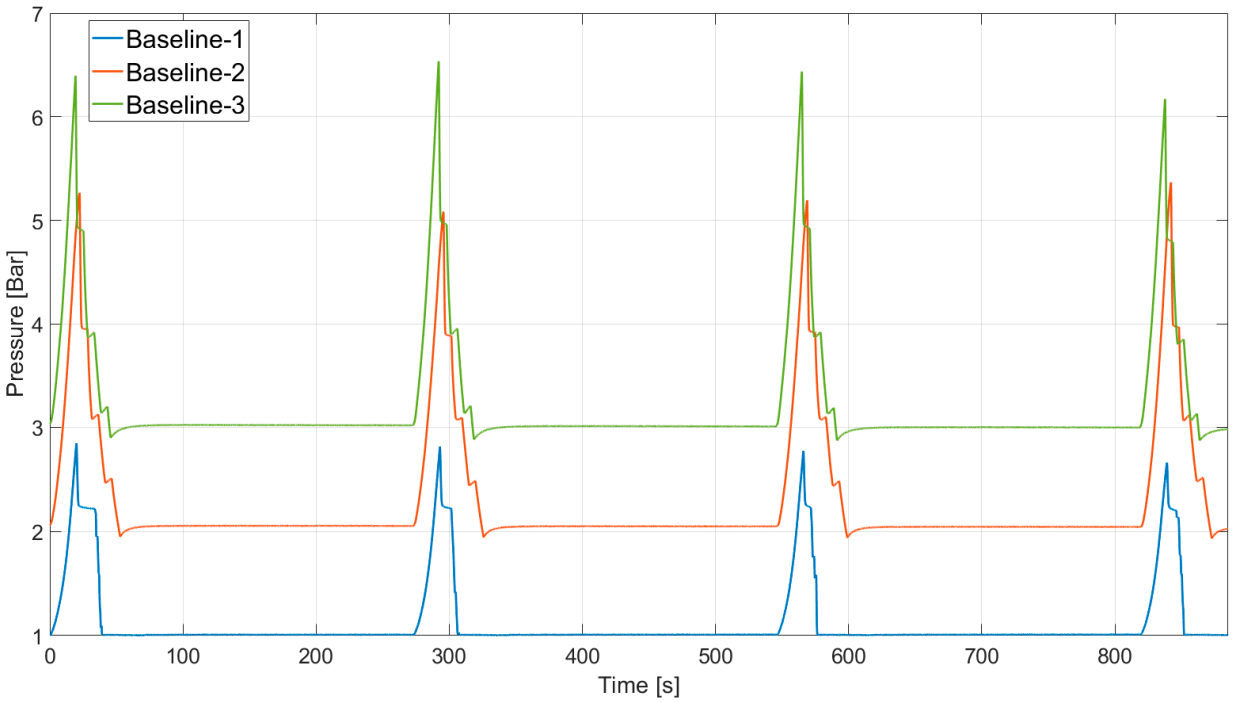
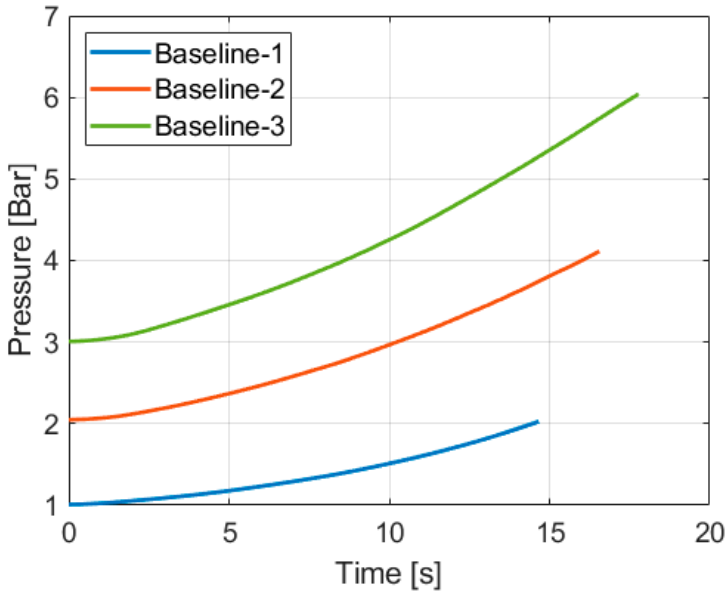
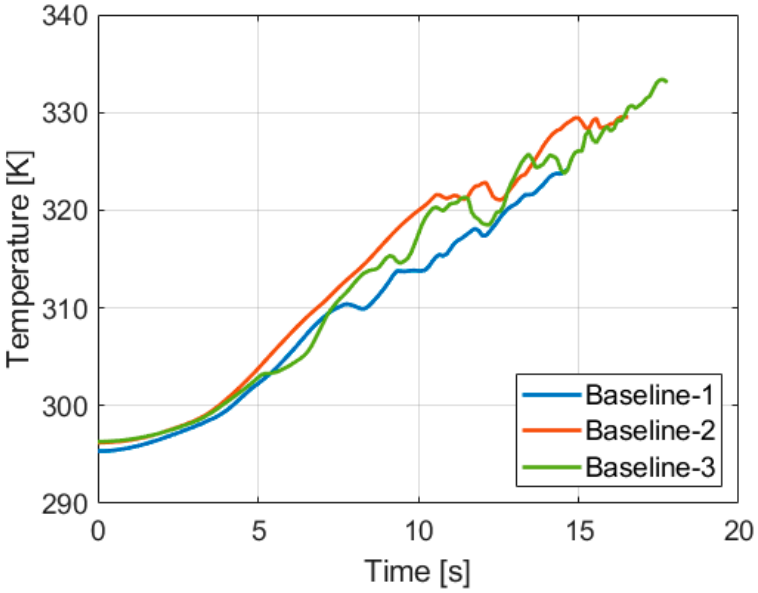


Figure 6. Pressure of entire cycle of baseline-1/2/3.

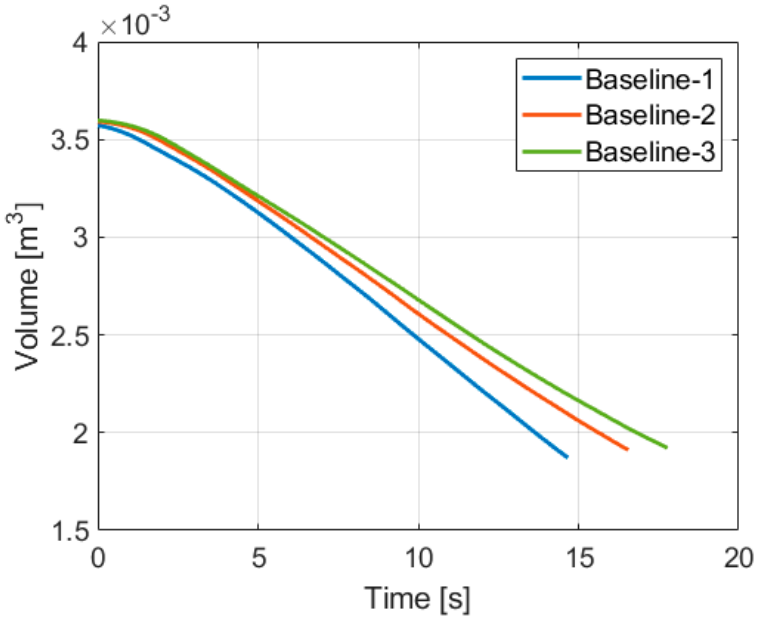


(**a**)

Figure 7. *Cont.*



(**b**)

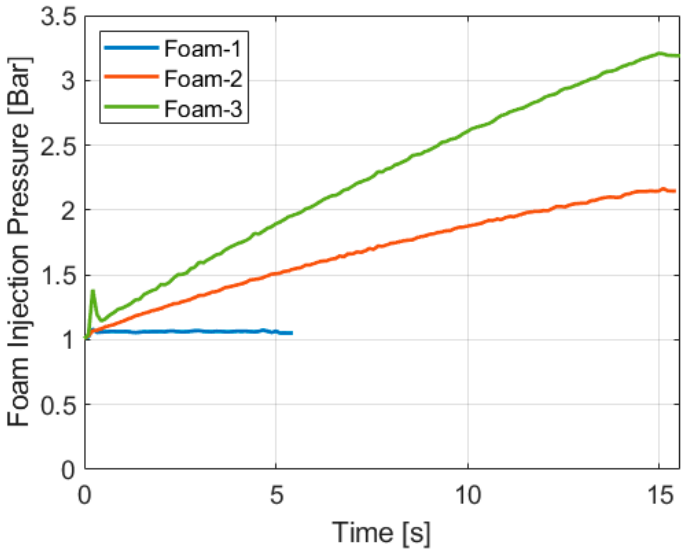


(**c**)

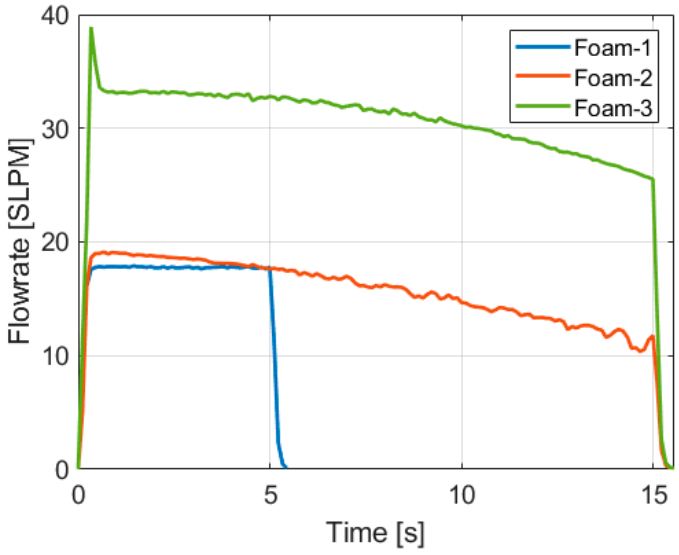
Figure 7. Air properties of baseline compression: (**a**) pressure, (**b**) temperature, (**c**) volume.

4.2. Compression with Aqueous Foam

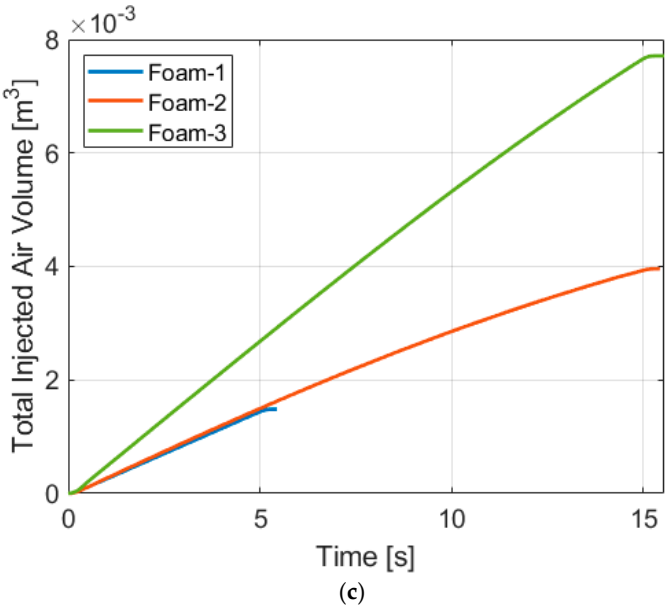
Figure 8 displays the properties of the air blown into the chamber to generate aqueous foam. The injection pressure, flowrate, and total volume of the injected air are presented in Figure 8a, b, and c, respectively. Figure 8a shows the pressure of the inlet air. For the pressure data, a pressure transducer was installed near the chamber inlet for the air-blowing source (sensor #2 beneath the chamber in Figure 4b system diagram). For Foam-1, because the chamber is open to the atmosphere, a minor increase in the inlet pressure is displayed, and it took only about five seconds to generate the intended amount of foam. For Foam-2 and 3, the air-blowing process was performed with the outlet closed to set up the initial pressure of 2 and 3 bars. Thus, continuous increase in the injection air pressure is shown, and the foam generation for Foam-2 and 3 took about 15 s. Figure 8b shows the flowrate of the blowing air, and Figure 8c shows the total volume of the injected air computed based on the flowrate.



(**a**)



(**b**)

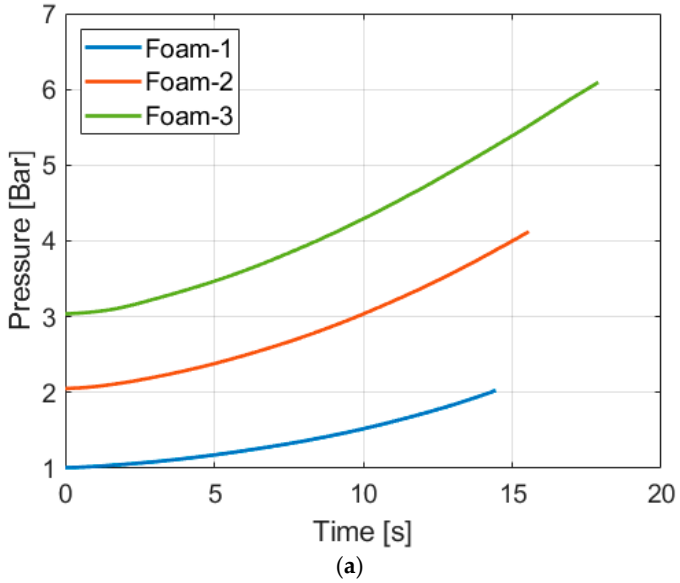


(**c**)

Figure 8. Foam-generating air conditions: (**a**) injection pressure, (**b**) flowrate, (**c**) total volume of foam-generating air.

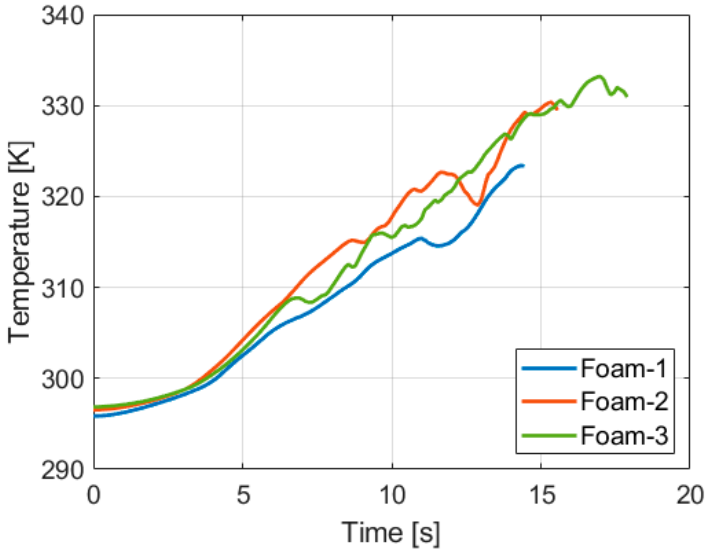
The flowrate of the blowing air used to generate aqueous foam is displayed in Figure 8b. This graph shows that Foam-1 required air injection for 5 s to reach the desired foam height. The flowrate for this trial was constant throughout the 5 s because the chamber was open to the atmosphere, allowing the addition of air to be unopposed. In contrast, Foam-2 and Foam-3 each took 15 s to generate the required foam levels. Throughout this time, both trials experienced a decrease in flowrate caused by the increasing pressure of the chamber. For Foam-2, the chamber began at 1 bar and was pressurized to 2 bars by the injected air. During this process, the flowrate decreased to about half of its original value, going from approximately 20 SLPM to 10 SLPM, due to the increasing pressure. As the pressure inside the chamber increased, there was more resistance to the addition of air, thus decreasing the rate at which the air was added to the chamber. Foam-3 underwent a similar process of flowrate decrease, from about 40 SLPM to 25 SLPM. Figure 8c displays the total volume of injected air added to the chamber's initial air volume of about 3.6×10^{-3} m^3. It can be observed that the total injected volume of air into the chamber is approximately the same as the initial volume for Foam-2, and two times for Foam-3. This is to be expected, as the pressure of the chamber is proportional to the amount of air molecules present in the chamber. Thus, to double the pressure of the chamber and achieve a pressure of 2 bars, the same amount of air as the chamber volume needs to be injected. Likewise, to achieve 3 bars, the total amount of air needs to be tripled, and the volume of the injected air needs to be twice as much as the chamber volume. Since the number of molecules is not the only factor that affects the pressure, the injected air volumes are not exact ratios of the initial air volume.

Compressions with aqueous foam were performed at 1 bar (Foam-1), 2 bars (Foam-2), and 3 bars (Foam-3), and the air properties of the processes are presented in Figure 9. The trends shown in the aqueous foam data observed in Figure 9 are similar to those of the baseline tests. It is observed that for a higher-pressure test, despite the slow compression, the temperature increases more than a lower-pressure test.

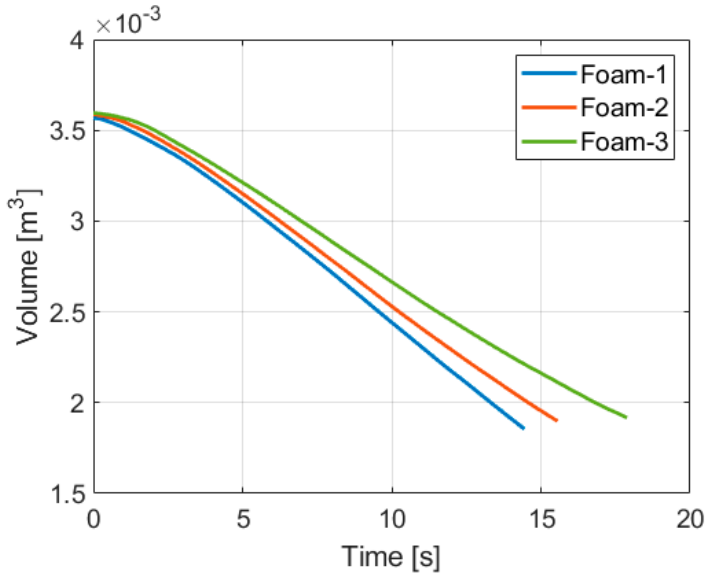


(**a**)

Figure 9. *Cont.*



(**b**)



(**c**)

Figure 9. Air properties of compression with aqueous foam: (**a**) pressure, (**b**) temperature, (**c**) volume.

Table 1 shows the temperature increases in all the tests. Comparing the two at the same pressure level, compression with the foam shows less temperature change than compression without the foam. Hence, the aqueous foam helps achieve the isothermal efficiency improvement. The results are compatible with the results presented in [36]. For both cases, the trend shows that a higher initial pressure leads to less isothermal performance.

Table 1. Temperature increases in Baseline-1/2/3 and Foam-1/2/3.

Temperature Increase [K]		
P_0 **[Bar]**	**Baseline**	**Foam**
1	28.90	27.47
2	33.32	32.95
3	36.75	34.08

4.3. Isothermal Efficiency of Compressions with and Without Aqueous Foam

The normalized pressure–volume profiles of the tests are given in Figure 10. The profiles of the baseline experiments are presented in Figure 10a, and the foam experiments in Figure 10b. To normalize, the pressure and volume data were divided by the initial value of the properties. For both tests, the profile of a lower initial pressure is located closer to the isothermal profile. This means that the isothermal performance of a lower-pressure compression is more efficient than a higher-pressure compression.

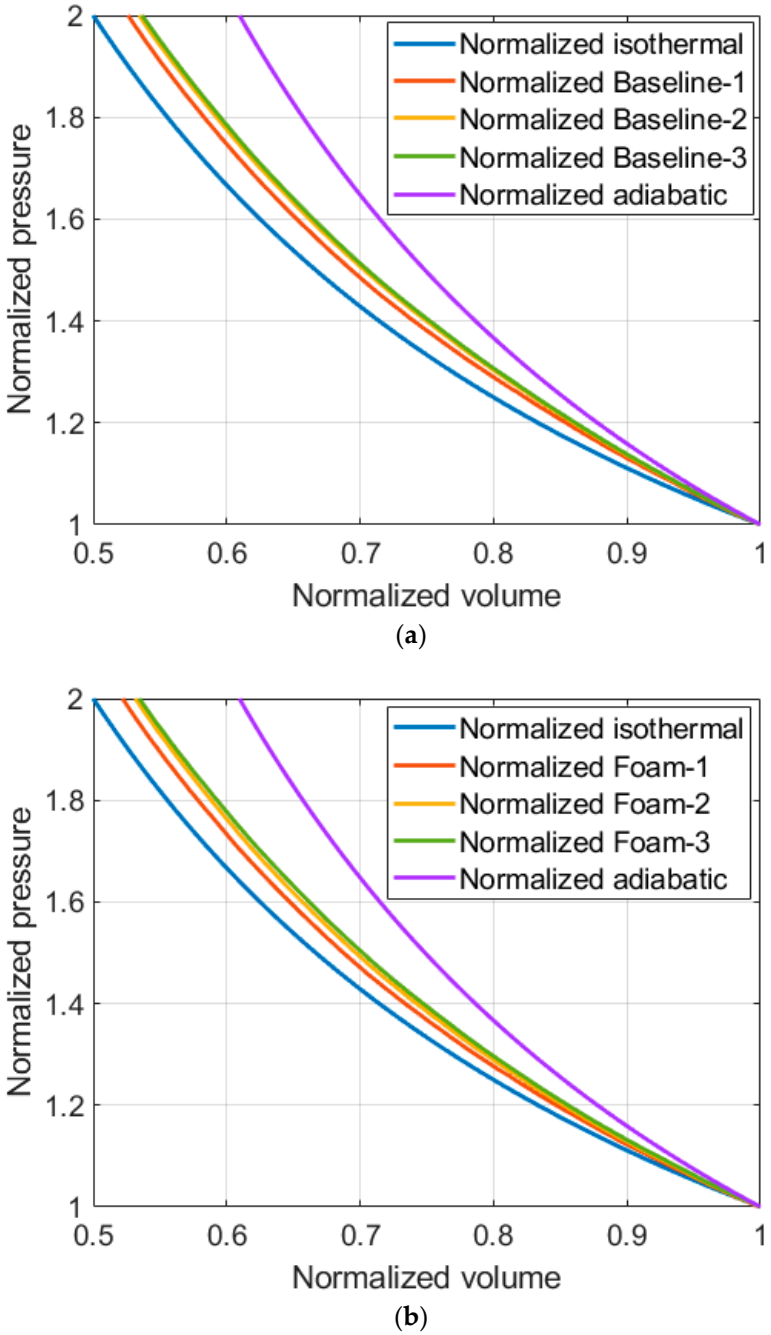


Figure 10. Normalized pressure–volume comparison with isothermal and adiabatic profiles: (**a**) Baseline-1/2/3, (**b**) Foam-1/2/3.

The isothermal efficiency of each process is computed with Equation (6) and is given in Table 2. The results agree with the isothermal performance evaluation based on the temperature results, in that the computed values are smaller with a higher initial pressure

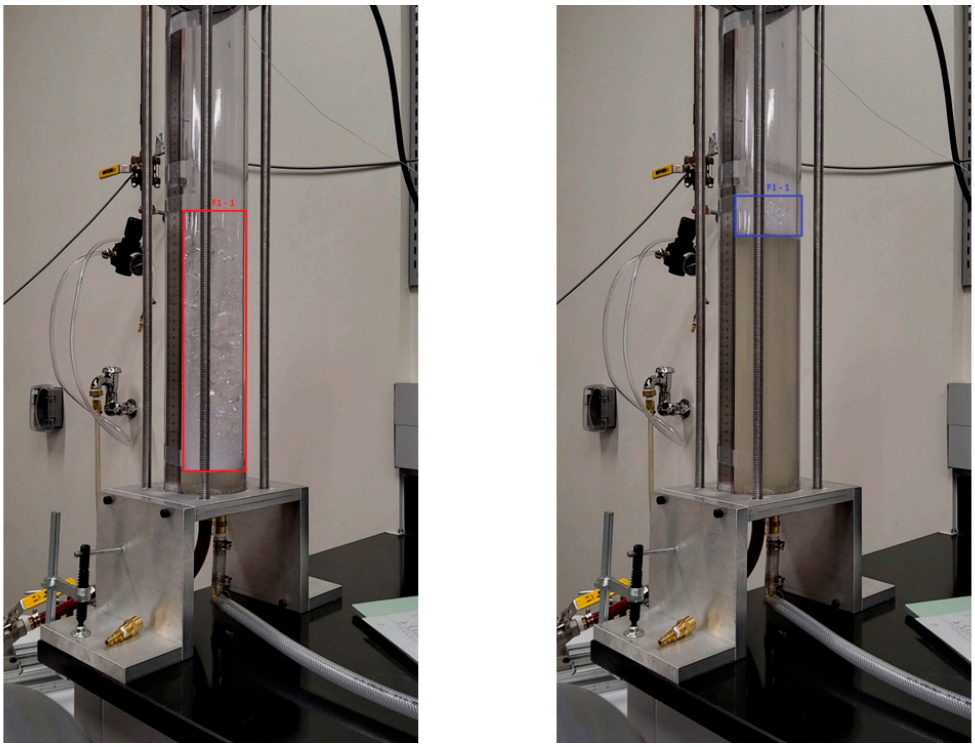
for both processes. Given that the thermocouple only measures the local temperature near its tip, and that there is a possibility of inadvertent liquid contact with the sensor, another performance evaluation with pressure–volume data helps verify the impacts of the foam and the initial pressures. The increment of the isothermal efficiency, $\Delta\eta_{iso}$, with the aid of the foam, is also given in Table 2. With the aid of the foam, efficiency improvement was observed at the three pressure levels; however, the efficiency gain from the foam decreases when the pressure level increases.

Table 2. Isothermal efficiency of Baseline-1/2/3 and Foam-1/2/3.

	Isothermal Efficiency [%]		
P_0	**Baseline**	**Foam**	$\Delta\eta_{iso}$
1 Bar	89.2	91.4	2.2
2 Bar	86.1	88.2	2.1
3 Bar	85.3	86.6	1.3

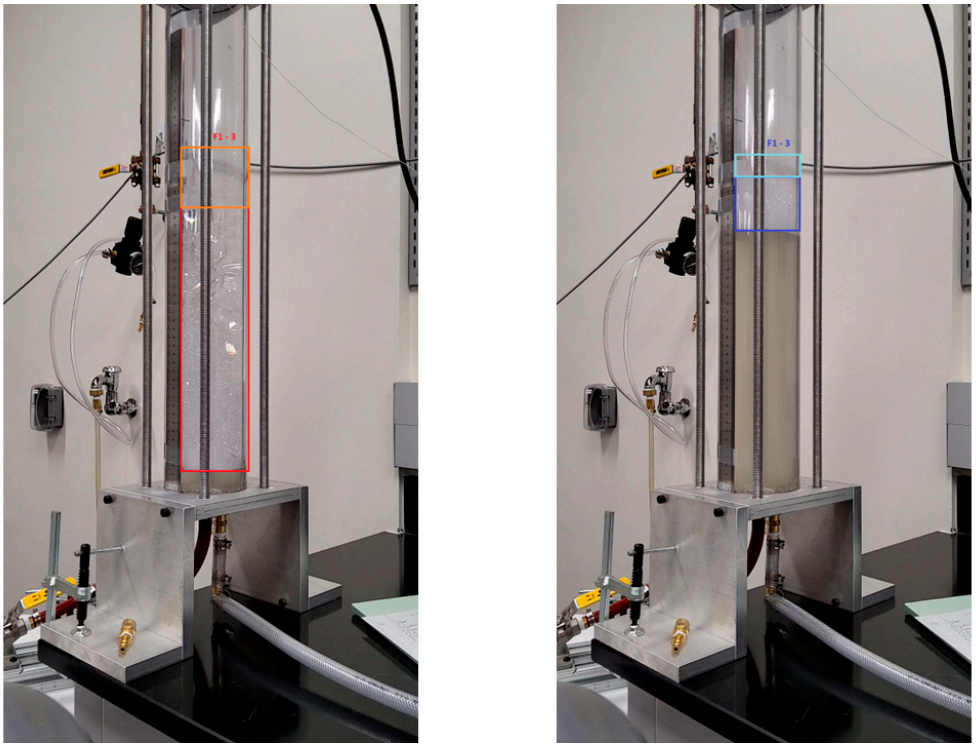
4.4. Aqueous Foam Results Analysis

The foam layer height change is shown in Figure 11. The volume of the foam filling the chamber is one of the factors that determines the isothermal efficiency [36]. Hence, observing the foam layer height changes may assist with understanding the efficiency differentiation at different pressure levels. Figure 11a shows a typical foam height change. The picture on the left is a before-compression state, and the one on the right is the point where the pressure ratio of 2 was reached. It is also important to note that not all bubbles fully collapse during compression, and some portion of foam stays around for the next stroke. The residual bubbles are faint and look different than normal bubbles. The residual foam is marked with a lighter colored box and is shown in Figure 11b.



(**a**)

Figure 11. *Cont.*



(**b**)

Figure 11. Foam layer height changes before and after compression. (**a**) shows the bubble height in red before the first compression stroke on the left and the bubble height in blue after the first compression on the right. (**b**) shows the residual bubble height in faint red before the next compression stroke on the left and the residual bubble height in faint blue after the next compression stroke on the right.

Table 3 displays the height of the aqueous foam before and after compression and the efficiency of each stroke. The pictures to visually aid in observing foam height changes are given in the Appendix A. When a residual foam layer is notable, an asterisk is placed next to the height values. For each cycle, the results show an increase in the initial and final foam heights as compression is repeated. This is presumed to be caused by the existence of residual bubbles that did not completely collapse in the previous stroke. Despite the variations, each stroke showed a similar isothermal efficiency under the same pressure conditions. The initial pressure and isothermal efficiency display an inversely proportional relationship throughout. Overall, the amount of foam loss is greater in a higher initial pressure test, shown by the bigger change in the foam height, ΔH. This is caused by the greater pressure and temperature changes in a higher-pressure test, causing the foam to disappear more easily. This is presumed to contribute to lower efficiency and smaller efficiency improvement at a higher-pressure level. The collapse of a greater portion of bubbles means the loss of a greater amount of heat transfer area.

As observed in Table 3, the foam volume conditions were not consistent. Except for the outliers with the asterisks, the chamber is filled with a greater amount of air in a higher-pressure case. This is because of the technical difficulties of generating aqueous foam while setting up initial pressure levels. To set up higher initial pressure, air injection at a higher pressure was required, which accompanies a higher flowrate of air. Thus, as displayed in Figure 8b, the flowrate at each pressure level differs from one another. However, this does not change the trend shown by the results. In [36], the impact of the size of bubbles due to different flowrates and the volume of the foam in the chamber on the isothermal efficiency was examined. A higher flowrate and a greater volume showed a higher isothermal efficiency. Thus, in the current experiments, a higher-pressure case was exposed to two advantageous conditions. Despite the beneficial conditions, lower isothermal efficiency

was observed at a higher pressure. Therefore, under consistent conditions, an efficiency decrease at a higher pressure could be more significant. Furthermore, considering the impact of those two conditions on isothermal efficiency is relatively marginal, it is safe to conclude that a higher initial condition leads to a lower isothermal efficiency.

Table 3. Isothermal efficiency, foam initial height, foam final height, and foam height changes in every stroke of compressions with aqueous foam (* case when residual foam height is notable).

Process	Stroke #	$H_{initial}$ [mm]	H_{final} [mm]	ΔH [mm]	η_{iso} [%]
Foam-1	1	300	45	255	91.23
	2	305	50	255	91.23
	3	375 *	85 *	290	91.87
Foam-2	1	330	85	245	87.87
	2	360	95	265	88.22
	3	375	110 *	265	88.48
Foam-3	1	365	45	320	86.50
	2	375	55	320	86.62
	3	385	65	320	86.72

4.5. Suggestion for Applications in Real System and for Future Work

In this subsection, how aqueous foam can be employed in a multi-stage compression system is suggested in an energy-saving manner. Even though there is no additional work input while the process is ongoing, generating foam ahead of the start of the process requires work input. However, this work input can be saved in a multi-stage compression system, and this mechanism is schematically illustrated in Figure 12.

Figure 12 displays a multi-stage liquid piston air compression system. Once air is compressed in Stage 1, the compressed air is transferred to Stage 2, where compression is performed at a higher-pressure level than the previous stage. Since the total volume of the air decreases after compression in Stage 1, a smaller number of liquid pistons is needed in Stage 2. In the present experimental work, unlike many liquid piston experimental studies that have used water as a liquid of the system, a soap solution was used as a liquid column of the system so that a simple air-blowing process through the liquid can directly generate the foam. This can be directly applied to a real system. By connecting the outlet of the first stage compressors to the bottom of the next stage chamber, the transferring process itself from a previous stage to the next stage functions as the air-blowing process for aqueous foam generation. Hence, the foam can be generated without an extra step, which may cause additional work input, in a higher-pressure stage. Despite the relatively small improvement in isothermal efficiency, this operation in an energy-saving manner can make aqueous foam a viable technique, particularly for a high-pressure-stage of a real system. For example, although the spray injection method can highly enhance the isothermal performance, it is hard to be employed in a higher-pressure stage. Because the spray work input is exponentially proportional to the pressure level, the overall efficiency including the spray work input showed a significantly lower value at a higher-pressure level [35]. Taking advantage of solid inserts is another approach to improve isothermal performance. However, the existence of inserts in the chamber compromises the initial volume of the chamber, and the expense for the materials to equip an actual large-scale system with solid inserts could be costly.

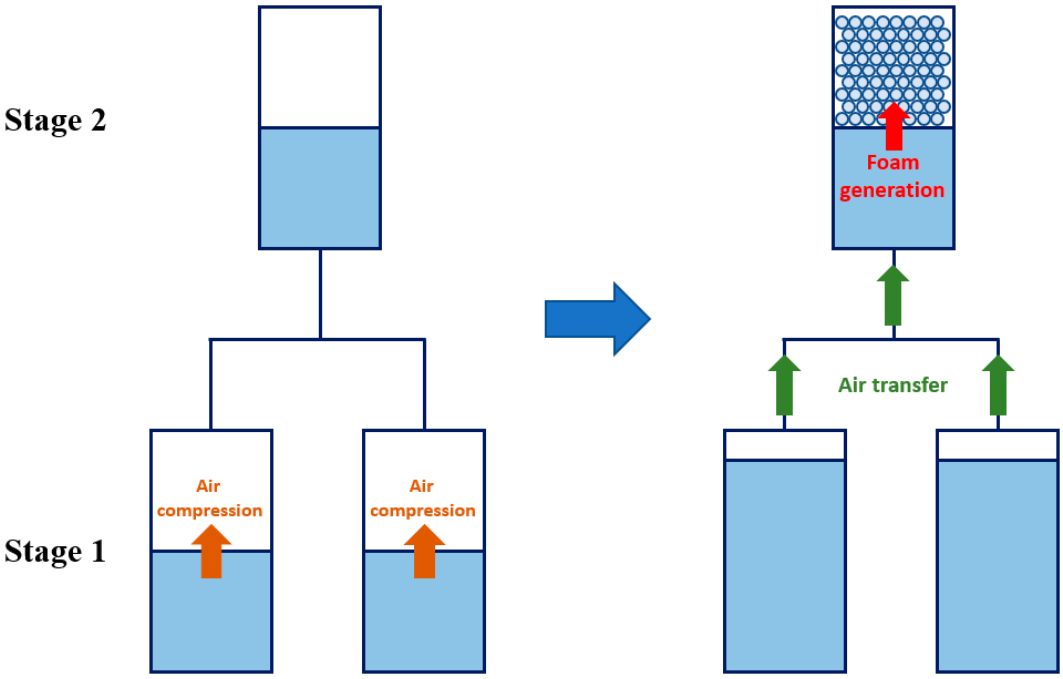


Figure 12. Aqueous foam generation in multi-stage compression system.

Despite the various pressure levels tested in the current experiments, the tested ranges of pressure were still relatively low in an effort to avoid extreme temperature/pressure conditions for the safe operation of the current setup with a transparent chamber that enables visual observation, which was a critical part of the analysis. Hence, to validate the aforementioned suggestion, testing aqueous foam in extreme pressure is required, and this can be a topic for future work.

5. Conclusions

In this article, aqueous foam is tested as a heat transfer enhancement agent in liquid piston gas compression. To examine its applicability to an actual CAES equipped with a multi-stage compression system, it needs to be tested at different initial pressures. Hence, compressions were performed at different initial pressure levels of 1, 2, and 3 bars, both with and without aqueous foam. Provided that the isothermal efficiencies of compressions starting at 1, 2, and 3 bars were 91.4%, 88.2%, and 86.6%, respectively, which are improved values compared to 89.2%, 86.1%, and 85.3% of isothermal efficiency without the foam, the following conclusions can be drawn:

- For all the three pressure levels, the use of aqueous foam aided in achieving a better isothermal efficiency.
- In both cases, a higher initial pressure led to a decreased efficiency.
- Efficiency improvement from the foam decreased as the initial pressure increased, even though the differences were marginal.

Considering that a higher-pressure case was exposed to more favorable conditions in the tests but showed a decreased efficiency, aqueous foam as a heat transfer booster seems less effective as the pressure level gets higher. To explore the reason for the variation in effectiveness, the foam volume changes were investigated. During a higher-pressure test, the greater amount of bubble collapse was observed. Hence, the less effectiveness at a higher pressure may be partly attributed to the larger loss of the foam, caused by the greater change in pressure and temperature. In reality, there may be other reasons including air dissolution at higher pressure levels [35,48], which was not part of this study.

In addition, a suggestion was made to utilize the aqueous foam technique in an energy-saving manner. In an actual multi-stage compression system, the air transferred to the next compression stage can function as an air-blowing process to generate aqueous foam. Hence, the technique can be simply employed without an additional step.

The current study is limited to relatively low compression speed to limit the amount of temperature rise during compression. However, in the future study, we will examine the effect of different compression speeds on isothermal efficiency both experimentally and numerically using spherical bubble models.

Author Contributions: Conceptualization, P.I.R. and B.A.; methodology, P.I.R. and B.A.; validation, B.A.; formal analysis, B.A. and M.S.; investigation, B.A. and M.S.; resources, P.I.R.; data curation, B.A. and M.S.; writing—original draft preparation, B.A.; writing—review and editing, M.S. and P.I.R.; visualization, B.A.; supervision, P.I.R.; project administration, P.I.R.; funding acquisition, P.I.R. All authors have read and agreed to the published version of the manuscript.

Funding: Internal funding from Baylor University in the form of startup funds was used for this project.

Informed Consent Statement: During the preparation of this work, the authors used ChatGPT 4.0 in order to check grammar and to improve readability of the article. After using this tool/service, the author reviewed and edited the content as needed and took full responsibility for the content of the publication. No human subject was involved in this study.

Data Availability Statement: Data generated in the studies will be made available upon request.

Acknowledgments: This research received no external funding but internal funding from Baylor University. Also, a substantial portion of this paper comes from the Ph.D. Thesis [51] of Barah Ahn titled "Comprehensive Experimental Investigation of Liquid Piston Gas Compression for Energy Storage Applications", successfully defended in December of 2023 at Baylor University.

Conflicts of Interest: The authors declare no conflict of interest.

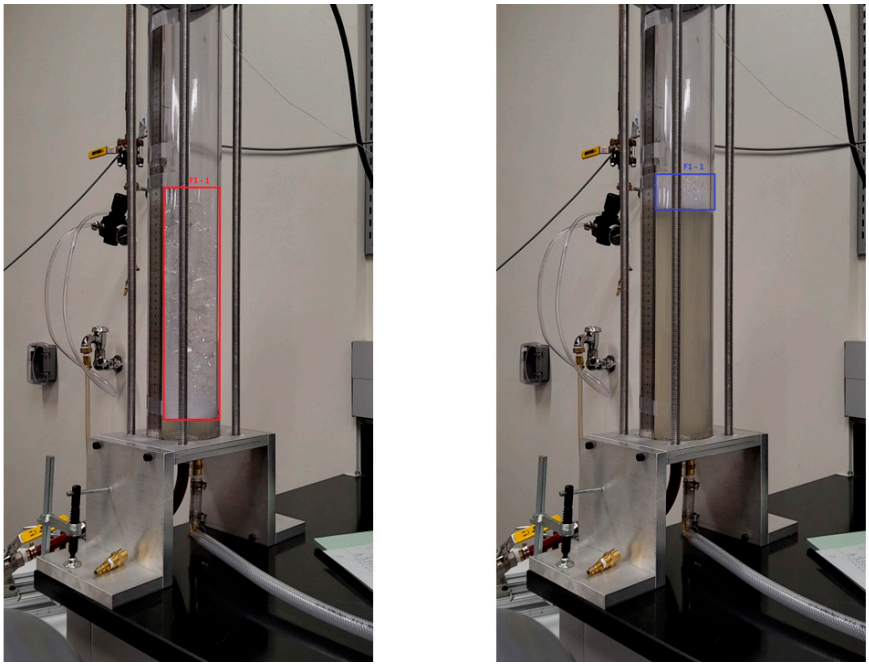
Abbreviations

Nomenclature

A_{foam}	Surface area of foam
A_s	Surface area
C_v	Specific heat
D_h	Hydraulic diameter
H_{final}	Final foam height
$H_{initial}$	Initial foam height
ΔH	Change in foam height
k_{foam}	Thermal conductivity of foam
L_{foam}	Thickness of single bubble
m_{air}	Mass of air
Nu_x	Nusselt number at entry
P	Pressure
P_0	Initial pressure
P_{air}	Pressure of air
P_f	Final pressure
P_{iso}	Pressure profile of isothermal process
Pr	Prandtl number
$\dot{Q}$	Rate of heat transfer
$\dot{Q}_{foam}$	Rate of aqueous foam heat transfer
$\dot{q}_{foam}$	Rate of heat transfer of single bubble
Re	Reynold number
T_{air}	Temperature of air

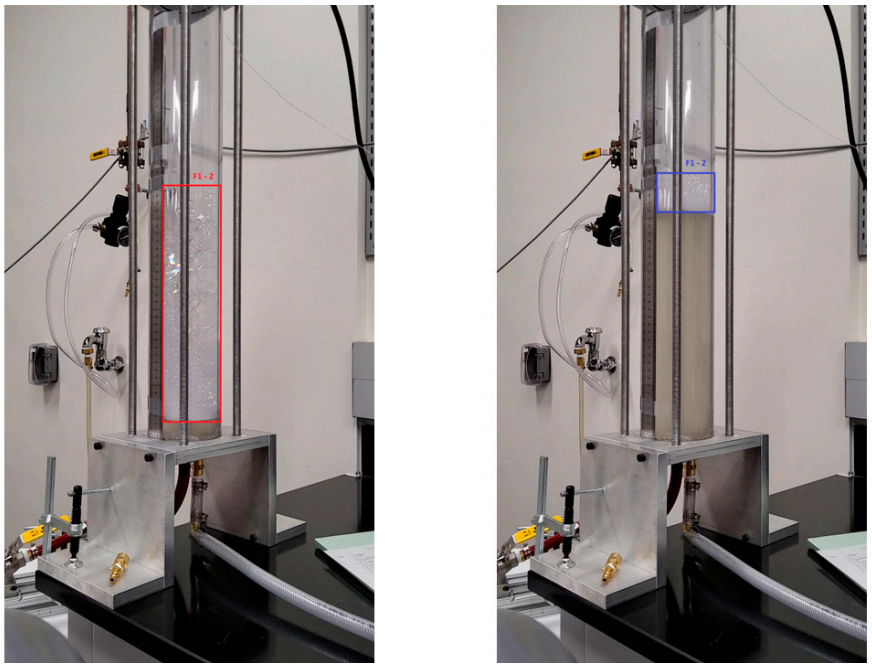
T_{foam}	Temperature of foam
T_{∞}	Temperature of surroundings
t	Time
U_h	Overall heat transfer coefficient
$\dot{U}$	Rate of internal energy
V	Volume
V_0	Initial volume
V_{air}	Volume of air
V_f	Final volume
$V_{f,iso}$	Final volume of isothermal process
V_{iso}	Volume profile of isothermal process
W_{comp}	Compression work
$W_{cooling}$	Cooling work
$W_{isothermal}$	Isothermal compression work
$\dot{W}_{compression}$	Rate of compression work
Greek letters	
η_{iso}	Isothermal compression efficiency
$\Delta\eta_{iso}$	Change in isothermal compression efficiency
Abbreviations	
CAES	Compressed air energy storage
A-CAES	Adiabatic compressed air energy storage
D-CAES	Diabatic compressed air energy storage
I-CAES	Isothermal compressed air energy storage
Baseline-1	Baseline compression starting at 1 bar
Baseline-2	Baseline compression starting at 2 bars
Baseline-3	Baseline compression starting at 3 bars
Foam-1	Compression with foam starting at 1 bar
Foam-2	Compression with foam starting at 2 bars
Foam-3	Compression with foam starting at 3 bars
PHS	Pumped hydroelectric storage

Appendix A

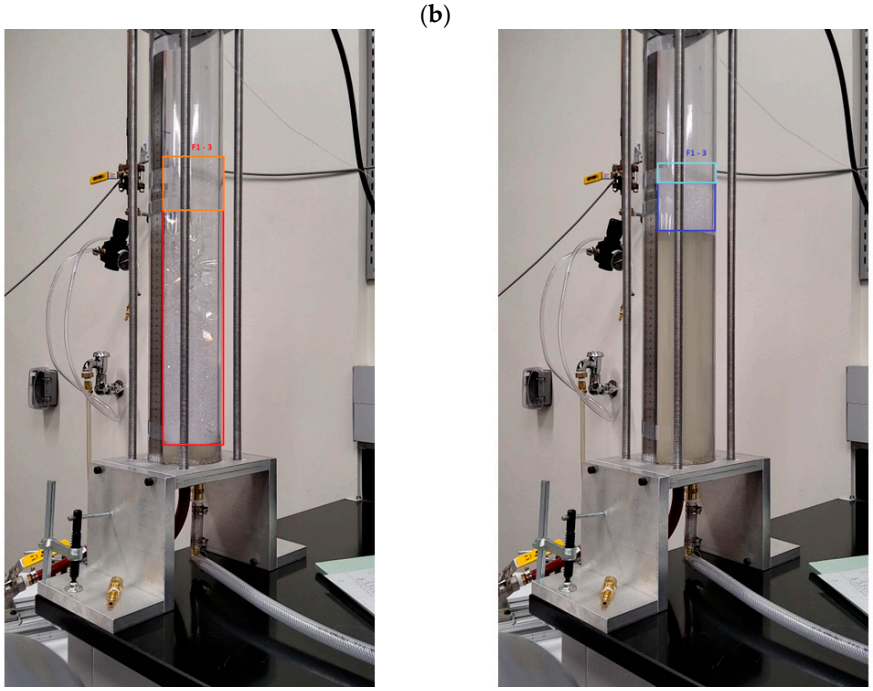


(**a**)

Figure A1. *Cont.*

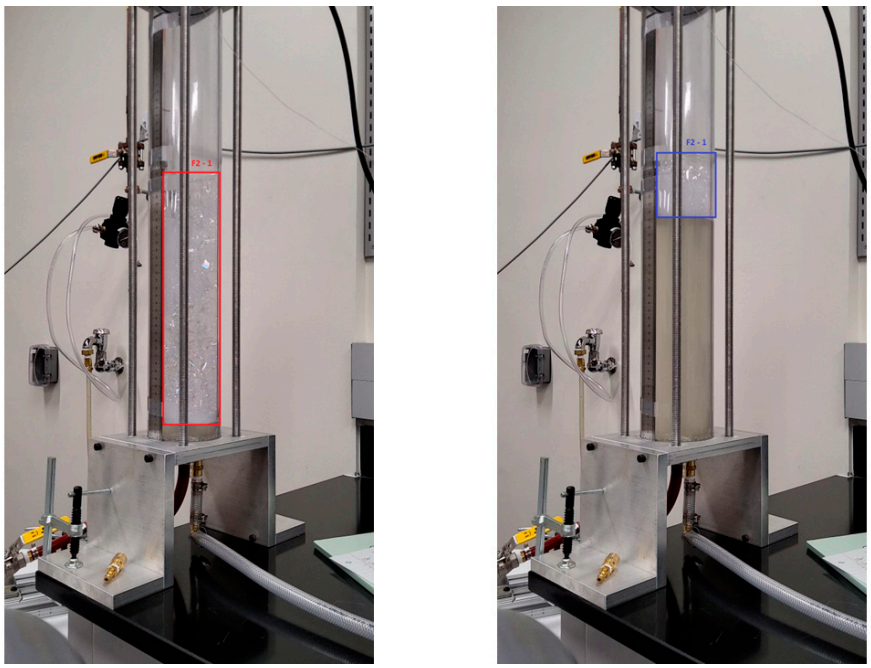


(**b**)

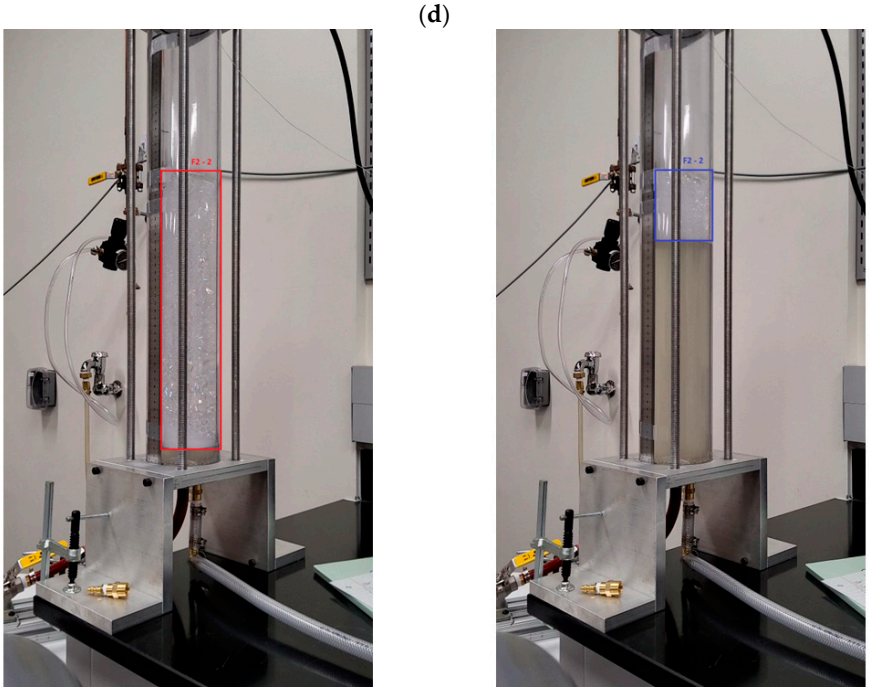


(**c**)

Figure A1. *Cont.*

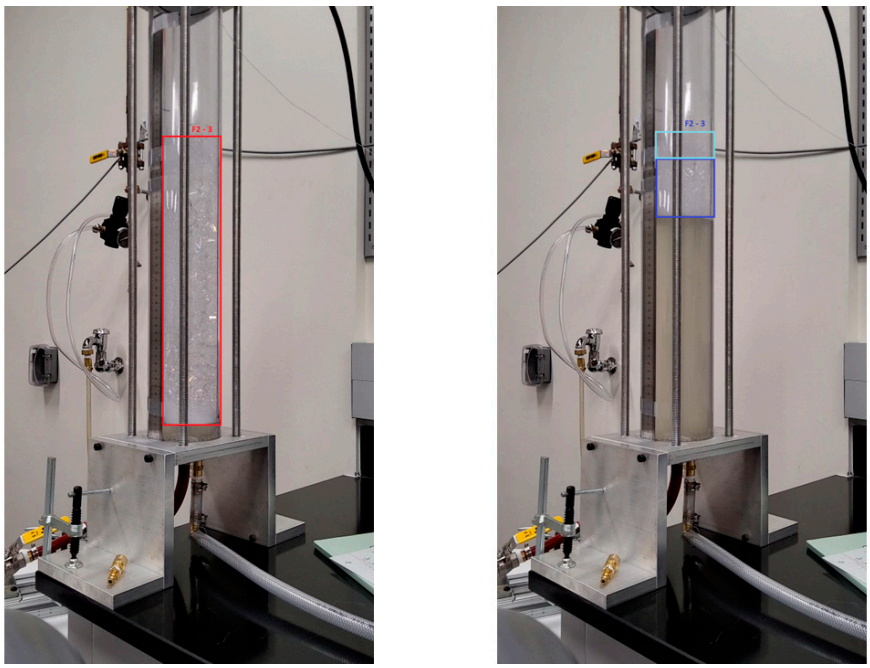


(**d**)

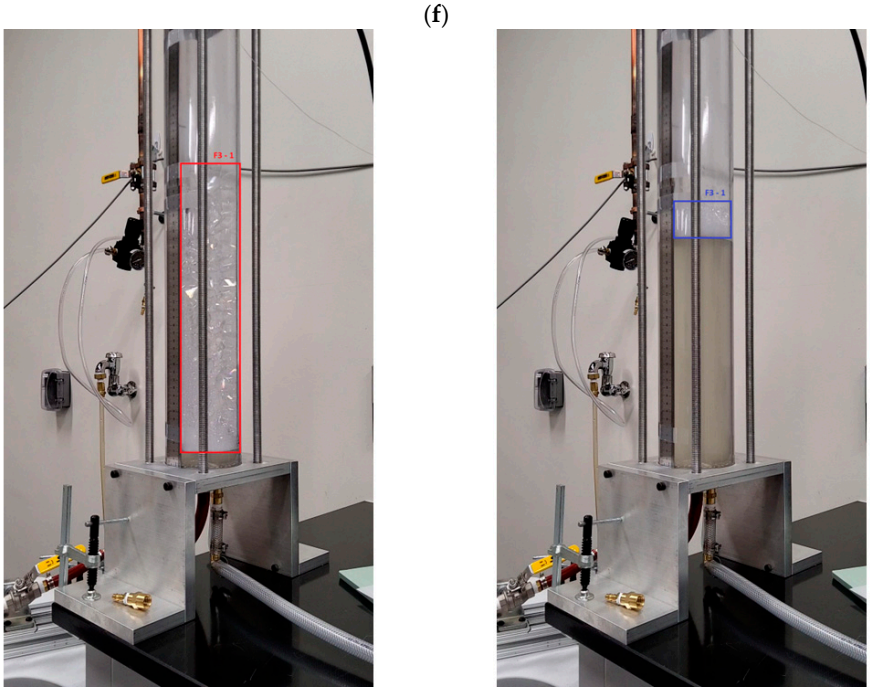


(**e**)

Figure A1. *Cont.*



(**f**)



(**g**)

Figure A1. *Cont.*

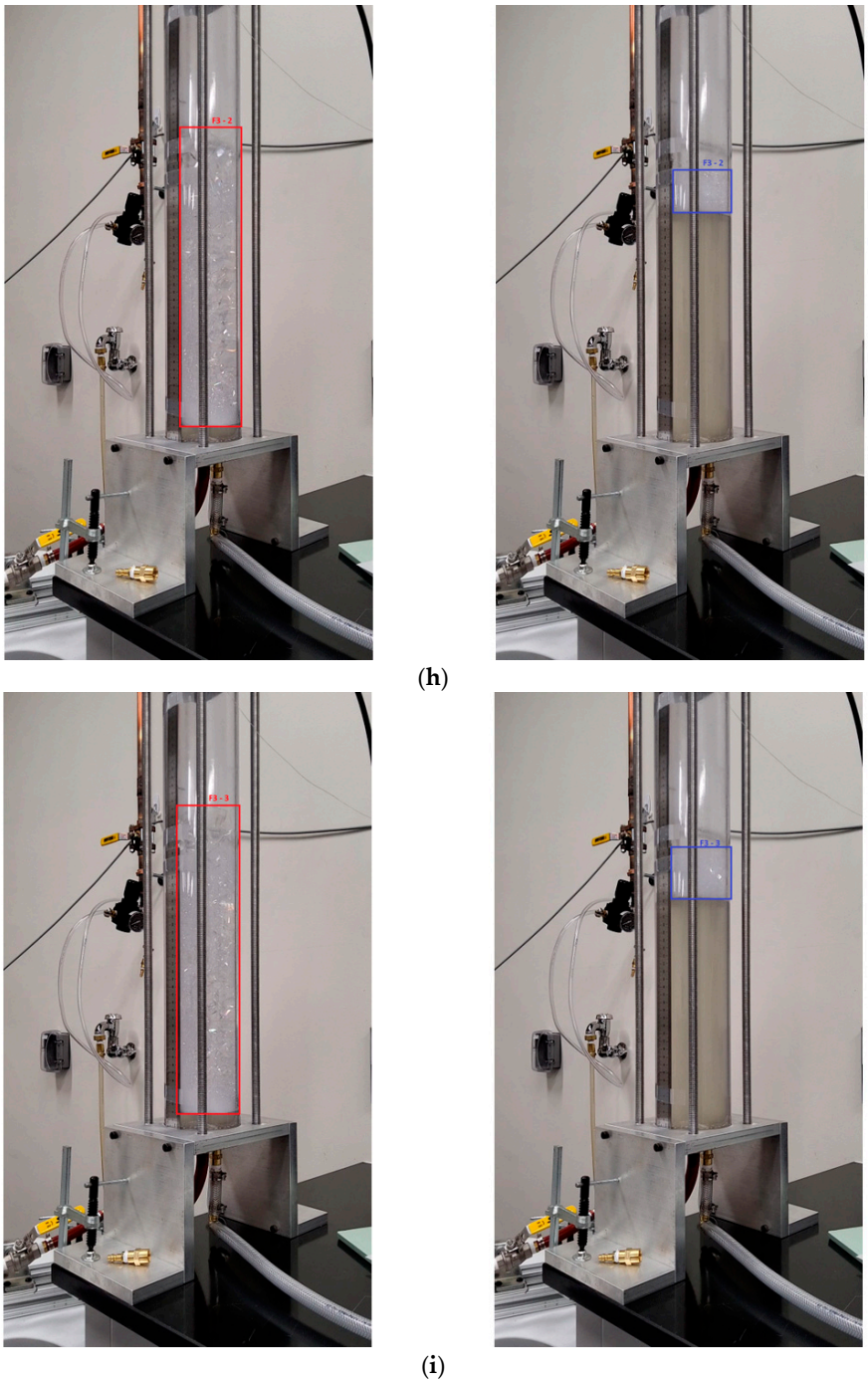


Figure A1. Foam height changes in (**a**) Foam-1 first stroke (**b**) Foam-1 second stroke (**c**) Foam-1 third stroke (**d**) Foam-2 first stroke (**e**) Foam-2 second stroke (**f**) Foam-2 third stroke (**g**) Foam-3 first stroke (**h**) Foam-3 second stroke (**i**) Foam-3 third stroke.

References

1. Fossil Fuels, EESI Environmental and Energy Study Institute. Available online: https://www.eesi.org/topics/fossil-fuels/description (accessed on 21 June 2023).
2. Frequently Asked Questions (FAQs)—What Is U.S. Electricity Generation by Energy Source? U.S. Energy Information Administration (EIA). Available online: https://www.eia.gov/tools/faqs/faq.php?id=427&t=3 (accessed on 21 June 2023).
3. Molina, F.; López, I.; Dapelo, D. A proposal to Make Frankfurt am Main Carbon Free by 2050. In *Technical Report for the Energy Transition in Frankfurt*; Provadis School of International Management and Technology: Frankfurt, Germany, 2013. [CrossRef]
4. YekiniSuberu, M.; Wazir Mustafa, M.; Bashir, N. Energy storage systems for renewable energy power sector integration and mitigation of intermittency. *Renew. Sustain. Energy Rev.* **2014**, *35*, 499–514. [CrossRef]

5. Qin, C.; Loth, E.; Li, P.; Simon, T.; Van de Ven, J. Spray-cooling concept for wind-based compressed air energy storage. *J. Renew. Sustain. Energy* **2014**, *6*, 043125. [CrossRef]
6. Wang, J.; Lu, K.; Ma, L.; Wang, J.; Dooner, M.; Miao, S.; Li, J.; Wang, D. Overview of compressed air energy storage and technology development. *Energies* **2017**, *10*, 991. [CrossRef]
7. Lim, S.D.; Mazzoleni, A.P.; Park, J.; Ro, P.I.; Quinlan, B. Conceptual Design of Ocean Compressed Air Energy Storage System. *Mar. Technol. Soc. J.* **2013**, *47*, 70–81. [CrossRef]
8. Evans, A.; Strezov, V.; Evans, T.J. Assessment of utility energy storage options for increased renewable energy penetration. *Renew. Sustain. Energy Rev.* **2012**, *16*, 4141–4147. [CrossRef]
9. Pemberton, D.; Jewitt, J.; Pletka, R.; Fischbach, M.; Meyer, T.; Ward, M.; Bjorge, B.; Hargreaves, D.; Jordan, G. *Mini-Compressed Air Energy Storage for Transmission Congestion Relief and Wind Shaping Applications*; New York State Energy Research and Development Authority: Albany, NY, USA, 2008.
10. Pimm, A.J.; Garvey, S.D.; de Jong, M. Design and testing of Energy Bags for underwater compressed air energy storage. *Energy* **2014**, *66*, 496–508. [CrossRef]
11. Bennett, J.A.; Simpson, J.G.; Qin, C.; Fittro, R.; Koenig, G.M.; Clarens, A.F.; Loth, E. Techno-economic analysis of offshore isothermal compressed air energy storage in saline aquifers co-located with wind power. *Appl. Energy* **2021**, *303*, 117587. [CrossRef]
12. Cavallo, A.J. Energy Storage Technologies for Utility Scale Intermittent Renewable Energy Systems. *J. Sol. Energy Eng.* **2001**, *123*, 387–389. [CrossRef]
13. Cavallo, A. Controllable and affordable utility-scale electricity from intermittent wind resources and compressed air energy storage (CAES). *Energy* **2007**, *32*, 120–127. [CrossRef]
14. Alirahmi, S.M.; Mousavi, S.B.; Razmi, A.R.; Ahmadi, P. A comprehensive techno-economic analysis and multi-criteria optimization of a compressed air energy storage (CAES) hybridized with solar and desalination units. *Energy Convers. Manag.* **2021**, *236*, 114053. [CrossRef]
15. Wolf, D. *Methods for Design and Application of Adiabatic Compressed Air Energy Storage Based on Dynamic Modeling*; Laufen: Oberhausen, Germany, 2011.
16. Tec-Science. Why Do Pressure and Temperature Increase During the Compression of a Gas? 2021. Available online: https://www.tec-science.com/thermodynamics/thermodynamic-processes-in-closed-systems/why-does-pressure-and-temperature-increase-during-the-compression-of-a-gas/ (accessed on 22 June 2023).
17. Kim, Y.-M.; Lee, J.-H.; Kim, S.-J.; Favrat, D. Potential and Evolution of Compressed Air Energy Storage: Energy and Exergy Analyses. *Entropy* **2012**, *14*, 1501–1521. [CrossRef]
18. Patil, V.C.; Ro, P.I. Energy and Exergy Analysis of Ocean Compressed Air Energy Storage Concepts. *J. Eng.* **2018**, *2018*, e5254102. [CrossRef]
19. Van de Ven, J.D.; Li, P.Y. Liquid piston gas compression. *Appl. Energy* **2009**, *86*, 2183–2191. [CrossRef]
20. Qin, C.; Loth, E. Liquid piston compression efficiency with droplet heat transfer. *Appl. Energy* **2014**, *114*, 539–550. [CrossRef]
21. Qin, C.C.; Loth, E. Isothermal compressed wind energy storage using abandoned oil/gas wells or coal mines. *Appl. Energy* **2021**, *292*, 116867. [CrossRef]
22. Patil, V.C.; Ro, P.I. Modeling of liquid-piston based design for isothermal ocean compressed air energy storage system. *J. Energy Storage* **2020**, *31*, 101449. [CrossRef]
23. Zhang, C.; Saadat, M.; Li, P.Y.; Simon, T.W. Heat Transfer in a Long, Thin Tube Section of an Air Compressor: An Empirical Correlation from CFD and a Thermodynamic Modeling. In *American Society of Mechanical Engineers Digital Collection*; American Society of Mechanical Engineers: New York, NY, USA, 2013; pp. 1601–1607. [CrossRef]
24. Zhang, C.; Li, P.Y.; Van de Ven, J.D.; Simon, T.W. Design analysis of a liquid-piston compression chamber with application to compressed air energy storage. *Appl. Therm. Eng.* **2016**, *101*, 704–709. [CrossRef]
25. Yan, B.; Wieberdink, J.; Shirazi, F.; Li, P.Y.; Simon, T.W.; Van de Ven, J.D. Experimental study of heat transfer enhancement in a liquid piston compressor/expander using porous media inserts. *Appl. Energy* **2015**, *154*, 40–50. [CrossRef]
26. Wieberdink, J.; Li, P.Y.; Simon, T.W.; Van de Ven, J.D. Effects of porous media insert on the efficiency and power density of a high pressure (210 bar) liquid piston air compressor/expander—An experimental study. *Appl. Energy* **2018**, *212*, 1025–1037. [CrossRef]
27. Ren, T.; Xu, W.; Cai, M.; Wang, X.; Li, M. Experiments on Air Compression with an Isothermal Piston for Energy Storage. *Energies* **2019**, *12*, 3730. [CrossRef]
28. Ren, T.; Xu, W.; Jia, G.-W.; Cai, M. A Novel Isothermal Compression Method for Energy Conservation in Fluid Power Systems. *Entropy* **2020**, *22*, 1015. [CrossRef] [PubMed]
29. Weiqing, X.; Ziyue, D.; Xiaoshuang, W.; Maolin, C.; Guanwei, J.; Yan, S. Isothermal piston gas compression for compressed air energy storage. *Int. J. Heat Mass Transf.* **2020**, *155*, 119779. [CrossRef]

30. Khaljani, M.; Vennard, A.; Harrison, J.; Surplus, D.; Murphy, A.; Mahmoudi, Y. Experimental and modelling analysis of efficiency enhancement in a liquid piston gas compressor using metal plate inserts for compressed air energy storage application. *J. Energy Storage* **2021**, *43*, 103240. [CrossRef]
31. Patil, V.C.; Liu, J.; Ro, P.I. Efficiency improvement of liquid piston compressor using metal wire mesh for near-isothermal compressed air energy storage application. *J. Energy Storage* **2020**, *28*, 101226. [CrossRef]
32. Patil, V.C.; Acharya, P.; Ro, P.I. Experimental investigation of water spray injection in liquid piston for near-isothermal compression. *Appl. Energy* **2020**, *259*, 114182. [CrossRef]
33. Ahn, B.; Patil, V.C.; Ro, P.I. Effect of Integrating Metal Wire Mesh with Spray Injection for Liquid Piston Gas Compression. *Energies* **2021**, *14*, 3723. [CrossRef]
34. Li, C.; Wang, H.; He, X.; Zhang, Y. Experimental and thermodynamic investigation on isothermal performance of large-scaled liquid piston. *Energy* **2022**, *249*, 123731. [CrossRef]
35. Ahn, B.; Ro, P.I. Spray cooling technique in liquid piston gas compression and impact of air dissolution on efficiency evaluation at different pressure levels. *J. Energy Storage* **2024**, *81*, 110460. [CrossRef]
36. Patil, V.C.; Ro, P.I. Experimental study of heat transfer enhancement in liquid piston compressor using aqueous foam. *Appl. Therm. Eng.* **2020**, *164*, 114441. [CrossRef]
37. Patil, V.C. *Efficiency Improvement Techniques in Liquid Piston Compressor for Ocean Compressed Air Energy Storage Application*; North Carolina State University: Raleigh, NC, USA, 2019.
38. Bollinger, B. *Demonstration of Isothermal Compressed Air Energy Storage to Support Renewable Energy Production*; SustainX, Inc.: Seabrook, NH, USA, 2015.
39. Wieberdink, J. *Increasing Efficiency and Power Density Of a Liquid Piston Air Compressor/Expander With Porous Media Heat Transfer Elements*; University of Minnesota: Minneapolis, MN, USA, 2014.
40. Marketwired, SustainX Begins Operating World's First Grid-Scale Isothermal Compressed Air Energy Storage System, Yahoo Finance. 2013. Available online: http://finance.yahoo.com/news/sustainx-begins-operating-worlds-first-130000557.html (accessed on 27 June 2023).
41. SustainX Delivers Compressed Air Energy Storage System, Nanalyze. 2014. Available online: https://www.nanalyze.com/2014/07/sustainx-delivers-compressed-air-energy-storage-system/ (accessed on 27 June 2023).
42. POWER. First Megawatt-Scale Isothermal CAES Completion, POWER Magazine. 2013. Available online: https://www.powermag.com/first-megawatt-scale-isothermal-caes-completion/ (accessed on 27 June 2023).
43. NRStor Advances CAES in Ontario, General Compression and SustainX Merges, Energy Storage World Forum. Available online: https://www.power-eng.com/energy-storage/long-duration-energy-storage/general-compression-sustainx-to-merge-as-gcx-energy-storage/ (accessed on 15 August 2025).
44. Attia, J.A.; McKinley, I.M.; Moreno-Magana, D.; Pilon, L. Convective heat transfer in foams under laminar flow in pipes and tube bundles. *Int. J. Heat Mass Transf.* **2012**, *55*, 7823–7831. [CrossRef] [PubMed]
45. Gylys, J.; Zdankus, T.; Gylys, M. Experimental investigation of heat transfer from inclined flat surface to aqueous foam. *Int. J. Heat Mass Transf.* **2014**, *69*, 230–236. [CrossRef]
46. Herzhaft, B. Rheology of Aqueous Foams: A Literature Review of Some Experimental Works. *Oil Gas Sci. Technol.—Rev. d'IFP Energies Nouv.* **1999**, *54*, 587–596. [CrossRef]
47. Larmignat, S.; Vanderpool, D.; Lai, H.K.; Pilon, L. Rheology of colloidal gas aphrons (microfoams). *Colloids Surfaces A: Physicochem. Eng. Asp.* **2008**, *322*, 199–210. [CrossRef]
48. Ahn, B.; Ro, P.I. Experimental Investigation of Impacts of Initial Pressure Levels on Compression Efficiency and Dissolution in Liquid Piston Gas Compression. *Energies* **2023**, *16*, 1921. [CrossRef]
49. Patil, V.C.; Acharya, P.; Ro, P.I. Experimental investigation of heat transfer in liquid piston compressor. *Appl. Therm. Eng.* **2019**, *146*, 169–179. [CrossRef]
50. Zhang, C.; Yan, B.; Wieberdink, J.; Li, P.; Van de Ven, J.; Loth, E.; Simon, T. Thermal analysis of a compressor for application to Compressed Air Energy Storage. *Appl. Therm. Eng.* **2014**, *73*, 1402–1411. [CrossRef]
51. Ahn, B. Comprehensive Experimental Investigation of Liquid Piston Gas Compression for Energy Storage Applications. Ph.D. Thesis, Baylor University, Waco, TX, USA, 2023.

Disclaimer/Publisher's Note: The statements, opinions and data contained in all publications are solely those of the individual author(s) and contributor(s) and not of MDPI and/or the editor(s). MDPI and/or the editor(s) disclaim responsibility for any injury to people or property resulting from any ideas, methods, instructions or products referred to in the content.